An improved rovibrational linelist of formaldehyde, H212C16O

An improved rovibrational linelist of formaldehyde, $H_2{}^{12}C^{16}O$

Afaf R. Al-Derzi[a], Jonathan Tennyson[1a], Sergei N. Yurchenko[a], Mattia Melosso[b], Ningjing Jiang[b], Cristina Puzzarini[b], Luca Dore[b], Tibor Furtenbacher[c], Roland Tóbiás[c], Attila G. Császár[c]

[a] *Department of Physics and Astronomy, University College London, Gower Street, London WC1E 6BT, United Kingdom*
[b] *Dipartimento di Chimica "Giacomo Ciamician", Università di Bologna, Via F. Selmi 2, 40126 Bologna, Italy*
[c] *MTA-ELTE Complex Chemical Systems Research Group and ELTE Eötvös Loránd University, Institute of Chemistry, Laboratory of Molecular Structure and Dynamics, H-1117 Budapest, Pázmány Péter sétány 1/A, Hungary*

Abstract

Published high-resolution rotation-vibration transitions of $H_2{}^{12}C^{16}O$, the principal isotopologue of methanal, are analyzed using the MARVEL (Measured Active Rotation-Vibration Energy Levels) procedure. The literature results are augmented by new, high-accuracy measurements of pure rotational transitions within the ground, ν_3, ν_4, and ν_6 vibrational states. Of the 16 596 non-redundant transitions processed, which come from 43 sources including the present work, 16 403 could be validated, providing 5029 empirical energy levels of $H_2{}^{12}C^{16}O$ with statistically well-defined uncertainties. All the empirical rotational-vibrational energy levels determined are used to improve the accuracy of ExoMol's AYTY line list for hot formaldehyde. The complete list of collated experimental transitions, the empirical energy levels determined, as well as the extended and improved line list are provided as Supplementary Material.

Keywords: Formaldehyde; Line list; Ro-vibrational energy; MARVEL analysis.

[1] To whom correspondence should be addressed; email: j.tennyson@ucl.ac.uk

1. Introduction

Formaldehyde, formally methanal, HCHO, is the simplest aldehyde. In the gas phase, formaldehyde is considered to be carcinogenic [1, 2]. Since formaldehyde is a trace species in the earth's atmosphere, formed as a result of photo-oxidation or through incomplete biomass burning, its carcinogenic nature motivated the development of spectroscopic techniques for detecting it in trace quantities [3].

The photochemistry and photophysics of formaldehyde, involving several excited electronic states and isomerization processes, leading to the products H_2 + CO or H + HCO, have been investigated in considerable detail [4–9], both experimentally and theoretically. The $\tilde{\mathrm{X}}\,^1A_1$ and $\tilde{\mathrm{A}}\,^1A_2$ electronic states of formaldehyde have been utilized in two-photon stimulated emission pumping (SEP) experiments to derive, for example, a complete set of 27 normal-mode vibrational constants characterizing the $\tilde{\mathrm{X}}\,^1A_1$ ground electronic state [10]. Thus, in 1984, Field and co-workers [10] could legitimately claim that the "unique characteristics of SEP have enabled us to describe the $E \leqslant 9300$ cm^{-1} rotation-vibration structure of H_2CO $\tilde{\mathrm{X}}\,^1A_1$ at a level of detail and completeness which we believe is without precedent for a four-atomic polyatomic molecule". Nevertheless, though a huge achievement, the accuracy attainable through these spectroscopic constants was a mere 3 cm^{-1}, hardly acceptable by present-day standards.

Over the years, beyond anharmonic (quartic) force field representations [11] of the $\tilde{\mathrm{X}}\,^1A_1$ PES of formaldehyde [12–15], several global PESs have been developed for the [C,H,H,O] system [9, 16–22]. Part of the interest in a global ground-electronic-state (S_0) PES stems from the existence of further important minima, *cis*- and *trans*-H–C–OH, hydroxycarbene [17, 20], on it besides that corresponding to formaldehyde. The *trans*-hydroxycarbene minimum is some 18 000 cm^{-1} [23] above the H_2CO minimum (the global minimum on S_0 belongs to CO + H_2 [23]), separated by a transition state of 10 400 cm^{-1}, measured from the hydroxycarbene side, and through enhanced deep tunneling *trans*-hydroxycarbene rearranges to formaldehyde with a half-life of only two hours [23]. The CO·H_2 complex has also been the topic of interesting dynamical and spectroscopic studies [24, 25].

Formaldehyde has been observed in different flames [26, 27], most famously in cold flames, first by Sir Humphry Davy [26] in 1817. The spectrum of formaldehyde has been used for its time-resolved monitoring in combustion engines [28], for which supporting spectroscopic studies have been performed [29].

Formaldehyde is a trace species on Mars [30], as well, and it is well known in comets [31–34]. Its

infrared absorption spectrum has been observed in protoplanetary disks [35]. Interstellar $H_2{}^{12}C^{16}O$ was detected 50 years ago [36] and many of the formaldehyde lines are now resolved routinely in high-resolution spectroscopic studies of the interstellar medium [37]. Interstellar formaldehyde masers have been widely observed [38–42].

Much of the laboratory spectroscopy of formaldehyde has focused on electronic (rovibronic) transitions. In fact, formaldehyde was the first polyatomic molecule where the rotational subband structure of vibronic transitions has been successfully analyzed [43]. It is probably fair to say that the photodissociation of formaldehyde is one of the most thoroughly understood polyatomic unimolecular reactions [6, 44].

The importance of line-by-line information on formaldehyde has led to a large number of laboratory studies of its high-resolution rotational-vibrational spectra [10, 28, 45–68, 68–107], involving a diverse set of experimental techniques, such as SEP [10], dispersed laser-induced fluorescence [75], conventional infrared spectroscopy, with some of the oldest results contained in Refs. [54, 57, 65, 67, 68], tunable infrared difference frequency laser spectroscopy [74], and sub-Doppler laser Stark and Doppler-limited Fourier-transform spectroscopy [79]. Many of the results of these high-resolution experimental studies will be addressed and discussed in detail below.

During the present study our focus is exclusively on transitions within the electronic ground state and we perform a MARVEL (Measured Active Rotational-Vibrational Energy Levels) [108–110] analysis of all the measured transitions of $H_2{}^{12}C^{16}O$ in its $\tilde{X}\,^1A_1$ state. This involves collating all available laboratory spectra and then validating the observed and assigned transitions. The collection of the validated lines is then inverted to give a set of accurate empirical energy levels with statistically significant associated uncertainties. As part of this study, the published spectra are augmented by high-accuracy measurements of pure rotational transitions within the ground, ν_3, ν_4, and ν_6 vibrational states.

Accurate energy levels have a number of uses in spectroscopy, kinetics, and thermochemistry. One of the opportunities is to improve theoretical prediction of rotation-vibration spectra [111]. Recently, as part of the ExoMol project [112], Al-Refaie *et al.* [113] computed an extensive rotation-vibration line list for hot formaldehyde, which they called AYTY. While this line list is comprehensive and reasonably accurate, its predicted line centers do not meet high resolution standards. The empirical energy levels generated, based partially on literature results and partially on the new measurements performed as part of this study, are used to make this line list suitable for high-resolution observational studies. This is achieved by a one-by-one replacement of the empirically

adjusted energy levels of the AYTY line list by the empirical rovibrational energy levels resulting from our MARVEL-based investigation. Such high-accuracy line lists are required, for example, by astronomers studying exoplanets using high-resolution Doppler-shift spectroscopy [114]. Indeed, experience shows that failed detections can in some cases be attributed to inaccurate line lists [115]. For this reason the ExoMol project decided to refactor its line lists to include empirically determined energy levels wherever possible [116]; this work forms part of this effort.

2. Methods

2.1. MARVEL

Details about the MARVEL technique [108–110], built upon the theory of spectroscopic networks (SNs) [117–119], and the xMARVEL code, introduced in Refs. 110 and 120, have been given in several recent publications [110, 118, 120–122]. MARVEL has been used to treat the laboratory

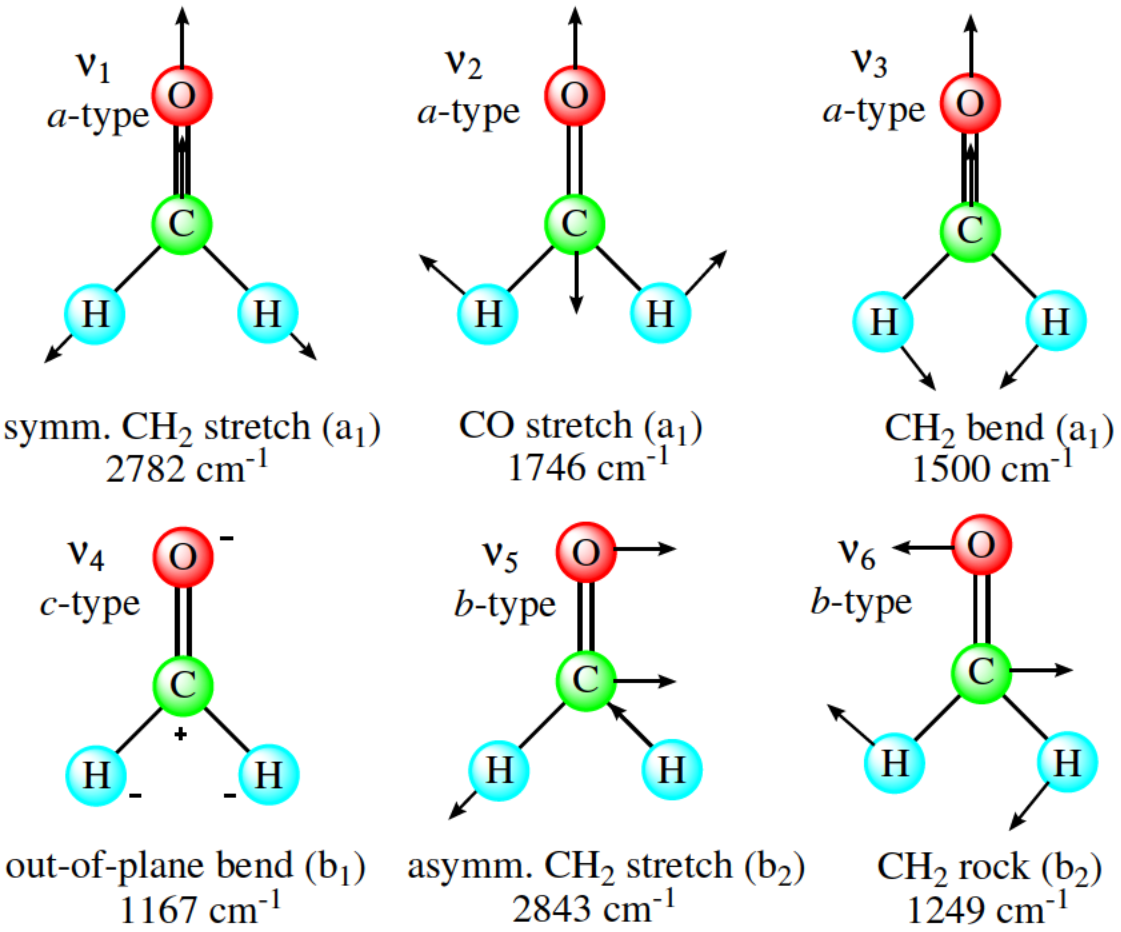

Figure 1: Vibrational fundamentals of $\tilde{X}\,^1A_1$ $H_2{}^{12}C^{16}O$, with their symmetry species and the types of bands indicated. The arrows representing atomic motions during the normal-mode vibrations are not proportional to the actual displacements.

spectroscopic data of nine isotopologues of water [111, 123–126], as well as of diatomics [127–131], triatomics [132–135], tetratomics [136–138], and beyond [139]. Thus, it is sufficient to give only a relatively brief discussion about MARVEL here.

Of importance to the present study, the MARVEL protocol yields empirical rovibronic energies with well-defined provenance and statistically-sound uncertainties. It always starts with the construction of a SN using the dataset of measured and assigned transitions collated from the literature. Then, a sophisticated inversion of the transitions is performed, yielding empirically determined rovibrational energy levels, with associated uncertainties, within each component of the SN. The inversion process expedites the validation of the experimental information through utilization of several elements of network theory.

The xMARVEL procedure [110, 120] has been used extensively during the present study to treat experimental rovibrational transitions of $H_2{}^{12}C^{16}O$. The corresponding xMARVEL input and output data files are provided as supplementary material.

2.2. Quantum numbers

The xMARVEL procedure requires as input spectral lines assigned with a unique set of quantum numbers. The equilibrium structure of formaldehyde on its ground electronic state has C_{2v} point-group symmetry (with irreducible representations, irreps, A_1, A_2, B_1, and B_2, which are the same for the isomorphic C_{2v}(M) molecular-symmetry group); it is an asymmetric-top, semirigid molecule. The vibration-rotation motions of formaldehyde can be well represented by a set of six vibrational normal-mode quantum numbers, $[v_1, v_2, v_3, v_4, v_5, v_6]$, arranged in standard order [140], and the three standard "rigid-rotor" quantum numbers [141], (J, K_a, K_c). See Fig. 1 for a pictorial representation of the normal modes of $H_2{}^{12}C^{16}O$. Rotational states with $K_a \approx J$ which differ only in their K_c quantum number lie close in energy and often give rise to two very-closely-spaced transitions, a phenomenon known as K-doubling or asymmetry splitting.

The electric-dipole-allowed transitions are described as $A_1 \longleftrightarrow A_2$ and $B_1 \longleftrightarrow B_2$. These selection rules are derived from symmetry relations. Namely, the two nuclear-spin isomers of $H_2{}^{12}C^{16}O$, *para* and *ortho*, correspond to $v_4 + v_5 + v_6 + K_a$ being even (irreps A) or odd (irreps B), respectively, while the subscripts of the irreps are 1 or 2 depending on whether $v_5 + v_6 + K_a + K_c$ is even or odd, respectively.

Table 1: Pure rotational Lamb-dip lines of $H_2{}^{12}C^{16}O$ measured during this study with 2 kHz (6.67×10^{-8} cm^{-1}) accuracy.[a]

$\sigma_{\rm new}$/cm^{-1}	Line assignment	$\sigma_{\rm lit}$/cm^{-1}
9.390 727 127	$\nu_0, 4_{1,4} \leftarrow 3_{1,3}$	9.390 727 53(33) [76]
9.694 153 448	$\nu_0, 4_{0,4} \leftarrow 3_{0,3}$	9.694 153 31(33) [76]
9.714 646 159	$\nu_0, 4_{2,3} \leftarrow 3_{2,2}$	9.714 646 7(67) [72]
		9.714 646 0(67) [76]
9.719 405 248	$\nu_0, 4_{3,2} \leftarrow 3_{3,1}$	9.719 407(10) [76]
9.719 536 101	$\nu_0, 4_{3,1} \leftarrow 3_{3,0}$	9.719 532 8(33) [85]
9.738 339 080	$\nu_0, 4_{2,2} \leftarrow 3_{2,1}$	9.738 339 0(67) [72]
10.034 829 847	$\nu_0, 4_{1,3} \leftarrow 3_{1,2}$	10.034 830 00(33) [76]

[a] In the first and last columns, the new, $\sigma_{\rm new}$, and the best previous, $\sigma_{\rm lit}$, transition wavenumbers are reported, respectively. The "Line assignment" column contains the assignments of the lines in the form of $\nu_0, J'_{K'_a,K'_c} \leftarrow J''_{K''_a,K''_c}$, where J_{K_a,K_c} denote the rotational assignment and ν_0 refers to the ground vibrational band both for the upper and the lower state.

2.3. New rotational measurements

In order to increase the number of available experimental data of $H_2{}^{12}C^{16}O$, and thus improve our MARVEL treatment, we have recorded a set of 89 pure rotational transitions in the ground and some vibrationally excited states. The measurements were performed using the frequency-modulation millimeter/submillimeter spectrometer in Bologna. The instrumental setup of the spectrometer is detailed elsewhere [142, 143]; here we provide only a brief description.

Table 2: Rotational lines of $H_2{}^{12}C^{16}O$ measured during this study with 20 kHz (6.67×10^{-7} cm^{-1}) accuracy.[a]

$\sigma_{\rm new}$/cm^{-1}	Line assignment	$\sigma_{\rm new}$/cm^{-1}	Line assignment	$\sigma_{\rm new}$/cm^{-1}	Line assignment
9.396 103 294	$\nu_3, 4_{1,4} \leftarrow 3_{1,3}$	12.098 165 470	$\nu_4, 5_{3,3} \leftarrow 4_{3,2}$	9.694 153 398	$\nu_0, 4_{0,4} \leftarrow 3_{0,3}$
9.720 532 400	$\nu_3, 4_{0,4} \leftarrow 3_{0,3}$	12.098 598 600	$\nu_4, 5_{3,2} \leftarrow 4_{3,1}$	9.714 646 044	$\nu_0, 4_{2,3} \leftarrow 3_{2,2}$
9.745 845 447	$\nu_3, 4_{2,3} \leftarrow 3_{2,2}$	12.129 667 850	$\nu_4, 5_{2,3} \leftarrow 4_{2,2}$	9.719 405 501	$\nu_0, 4_{3,2} \leftarrow 3_{3,1}$
9.753 700 377	$\nu_3, 4_{3,2} \leftarrow 3_{3,1}$	12.432 459 250	$\nu_4, 5_{1,4} \leftarrow 4_{1,3}$	9.719 535 726	$\nu_0, 4_{3,1} \leftarrow 3_{3,0}$
9.753 859 167	$\nu_3, 4_{3,1} \leftarrow 3_{3,0}$	9.366 709 450	$\nu_6, 4_{1,4} \leftarrow 3_{1,3}$	9.738 339 087	$\nu_0, 4_{2,2} \leftarrow 3_{2,1}$
9.773 007 973	$\nu_3, 4_{2,2} \leftarrow 3_{2,1}$	9.682 101 847	$\nu_6, 4_{0,4} \leftarrow 3_{0,3}$	9.834 452 846	$\nu_0, 22_{2,20} \leftarrow 23_{0,23}$
10.088 575 460	$\nu_3, 4_{1,3} \leftarrow 3_{1,2}$	9.697 356 479	$\nu_6, 4_{2,3} \leftarrow 3_{2,2}$	10.034 829 710	$\nu_0, 4_{1,3} \leftarrow 3_{1,2}$
11.739 822 940	$\nu_3, 5_{1,5} \leftarrow 4_{1,4}$	9.696 151 729	$\nu_6, 4_{3,2} \leftarrow 3_{3,1}$	10.248 367 590	$\nu_0, 9_{2,7} \leftarrow 10_{0,10}$
12.129 667 850	$\nu_3, 5_{0,5} \leftarrow 4_{0,4}$	9.696 255 862	$\nu_6, 4_{3,1} \leftarrow 3_{3,0}$	10.364 365 470	$\nu_0, 18_{3,15} \leftarrow 19_{1,18}$
12.178 445 400	$\nu_3, 5_{2,4} \leftarrow 4_{2,3}$	9.718 870 594	$\nu_6, 4_{2,2} \leftarrow 3_{2,1}$	10.448 342 040	$\nu_0, 37_{4,33} \leftarrow 37_{4,34}$
12.192 149 190	$\nu_3, 5_{4,2} \leftarrow 4_{4,1}$	10.029 447 240	$\nu_6, 4_{1,3} \leftarrow 3_{1,2}$	10.555 863 330	$\nu_0, 11_{1,10} \leftarrow 11_{1,11}$
12.192 149 190	$\nu_3, 5_{4,1} \leftarrow 4_{4,0}$	11.704 713 210	$\nu_6, 5_{1,5} \leftarrow 4_{1,4}$	10.896 074 830	$\nu_0, 19_{2,17} \leftarrow 19_{2,18}$
12.194 013 170	$\nu_3, 5_{3,3} \leftarrow 4_{3,2}$	12.086 508 690	$\nu_6, 5_{0,5} \leftarrow 4_{0,4}$	11.212 427 070	$\nu_0, 28_{3,25} \leftarrow 28_{3,26}$
12.194 571 510	$\nu_3, 5_{3,2} \leftarrow 4_{3,1}$	12.120 488 600	$\nu_6, 5_{2,4} \leftarrow 4_{2,3}$	11.733 738 380	$\nu_0, 5_{1,5} \leftarrow 4_{1,4}$
12.232 626 840	$\nu_3, 5_{2,3} \leftarrow 4_{2,2}$	12.109 817 660	$\nu_6, 5_{4,2} \leftarrow 4_{4,1}$	12.073 937 490	$\nu_0, 8_{2,6} \leftarrow 9_{0,9}$

Continued on next page

Table 2 – *Continued from previous page*

$\sigma_{\rm new}/{\rm cm}^{-1}$	Line assignment	$\sigma_{\rm new}/{\rm cm}^{-1}$	Line assignment	$\sigma_{\rm new}/{\rm cm}^{-1}$	Line assignment
12.604 848 190	$\nu_3, 5_{1,4} \leftarrow 4_{1,3}$	12.109 817 660	$\nu_6, 5_{4,1} \leftarrow 4_{4,0}$	12.099 570 770	$\nu_0, 5_{0,5} \leftarrow 4_{0,4}$
9.384 944 381	$\nu_4, 4_{1,4} \leftarrow 3_{1,3}$	12.121 054 530	$\nu_6, 5_{3,3} \leftarrow 4_{3,2}$	12.139 927 050	$\nu_0, 5_{2,4} \leftarrow 4_{2,3}$
9.649 643 518	$\nu_4, 4_{0,4} \leftarrow 3_{0,3}$	12.121 422 250	$\nu_6, 5_{3,2} \leftarrow 4_{3,1}$	12.145 176 040	$\nu_0, 5_{4,2} \leftarrow 4_{4,1}$
9.670 558 195	$\nu_4, 4_{2,3} \leftarrow 3_{2,2}$	12.163 422 430	$\nu_6, 5_{2,3} \leftarrow 4_{2,2}$	12.145 176 040	$\nu_0, 5_{4,1} \leftarrow 4_{4,0}$
9.677 770 970	$\nu_4, 4_{3,2} \leftarrow 3_{3,1}$	12.532 770 930	$\nu_6, 5_{1,4} \leftarrow 4_{1,3}$	12.150 912 170	$\nu_0, 5_{3,3} \leftarrow 4_{3,2}$
9.677 893 765	$\nu_4, 4_{3,1} \leftarrow 3_{3,0}$	8.237 600 872	$\nu_0, 21_{2,19} \leftarrow 22_{0,22}$	12.151 369 510	$\nu_0, 5_{3,2} \leftarrow 4_{3,1}$
9.693 290 175	$\nu_4, 4_{2,2} \leftarrow 3_{2,1}$	8.600 996 014	$\nu_0, 35_{3,32} \leftarrow 36_{1,35}$	12.187 211 040	$\nu_0, 5_{2,3} \leftarrow 4_{2,2}$
9.949 961 352	$\nu_4, 4_{1,3} \leftarrow 3_{1,2}$	8.615 829 497	$\nu_0, 10_{2,8} \leftarrow 11_{0,11}$	12.441 481 610	$\nu_0, 12_{1,11} \leftarrow 12_{1,12}$
11.726 529 220	$\nu_4, 5_{1,5} \leftarrow 4_{1,4}$	8.798 468 478	$\nu_0, 36_{4,32} \leftarrow 36_{4,33}$	12.538 447 510	$\nu_0, 5_{1,4} \leftarrow 4_{1,3}$
12.045 134 760	$\nu_4, 5_{0,5} \leftarrow 4_{0,4}$	8.815 102 825	$\nu_0, 10_{1,9} \leftarrow 10_{1,10}$	12.795 269 680	$\nu_0, 20_{2,18} \leftarrow 20_{2,19}$
12.084 311 370	$\nu_4, 5_{2,4} \leftarrow 4_{2,3}$	9.160 256 575	$\nu_0, 18_{2,16} \leftarrow 18_{2,17}$		
12.093 976 360	$\nu_4, 5_{4,2} \leftarrow 4_{4,1}$	9.390 727 004	$\nu_0, 4_{1,4} \leftarrow 3_{1,3}$		
12.093 936 030	$\nu_4, 5_{4,1} \leftarrow 4_{4,0}$	9.461 197 252	$\nu_0, 27_{3,24} \leftarrow 27_{3,25}$		

[a] $\sigma_{\rm new}$ denotes newly measured transition wavenumbers. The line assignments are given in the form of $\nu_i, J'_{K'_a,K'_c} \leftarrow J''_{K''_a,K''_c}$, where ν_i and J_{K_a,K_c} represent the vibrational and the rotational assignment of the measured lines, respectively, ν_0 refers to the ground vibrational state, while ν_3, ν_4, and ν_6 designate vibrational fundamentals (see Fig. 1).

The radiation source is a Gunn diode (80–115 GHz) that is frequency- and phase-stabilized *via* a phase-lock-loop and is driven by a centimeter-wave synthesizer referenced to a 5 MHz rubidium atomic clock. Spectral coverage between 240 and 420 GHz is obtained by coupling the Gunn diode to passive multipliers. Then, the electromagnetic radiation is frequency-modulated at $f = 48$ kHz and fed into a glass absorption cell (3 m optical path length) filled with formaldehyde vapors at pressure between 0.5 and 20 μbar; specifically, pressures between 0.5 and 20 μbar were used to record ground state lines with intensities spanning almost six orders of magnitude, while 10–15 μbar were used to observe the vibrational excited states. The sample of H_2CO was freshly obtained before each measurement from the vapors of solid, room-temperature paraformaldehyde. The output radiation was finally detected by a Schottky barrier diode, demodulated by a lock-in amplifier set at twice the modulation-frequency ($2f$ scheme), filtered, and analog-to-digitally converted.

A small sub-set of measurements have been performed exploiting the Lamb-dip technique [144]. In this respect, the optics of the spectrometer were adequately set up in a double-pass configuration (as detailed in [145]), f was set to 1 kHz, and a low-pressure of H_2CO was used (0.5 μbar).

The new measurements consist of (a) two complete a-type ${}^qR$-branch transitions ($J = 4 \leftarrow 3$ and $5 \leftarrow 4$) within the ν_0, ν_3, ν_4, and ν_6 bands, where ν_0 denotes the ground vibrational state, and (b) about 20 ground-state P and Q transitions with $\Delta K_a = 0$ or 2, with integrated intensity

between 10^{-23} and 10^{-27} cm molecule^{-1}.

The uncertainty of our measurements is estimated to be in the range of 2–20 kHz. We label the seven Lamb-dip transitions of Table 1 with the reference tag 21AlTeYuMe, and the others as 21AlTeYuMe_S2, see Table 2.

2.4. Artificial transitions

In the absence of transitions linking the *ortho* and *para* nuclear-spin isomers, the measured transitions form two distinct principal components (PC) [118] in the SN of $H_2{}^{12}C^{16}O$. As usual [111] during MARVEL analyses of experimental transitions of species having more than one nuclear-spin isomer, the *ortho* and *para* principal components are linked using artificial transitions, colloquially called magic numbers, taken possibly from effective Hamiltonian fits (EH) [122].

For $H_2{}^{12}C^{16}O$, the wavenumber of the unmeasurable rotational transition $1_{1,1} \leftarrow 0_{0,0}$, reported in [146] as 10.539 039 1 cm^{-1}, is utilized as a magic number. Since the very accurate empirical (MARVEL) energies of the pure rotational states $1_{0,1}$, $2_{0,2}$, and $3_{0,3}$, that is, 2.429 612 60(33), 7.286 404 28(47), and 14.565 513 07(58) cm^{-1}, respectively, are reproduced by the EH-predicted values, see the fourth column of Table 3 of Ref. [146], with unsigned deviations of 8.26×10^{-7}, 2.20×10^{-6}, and 4.37×10^{-6} cm^{-1}, respectively, the average of these unsigned deviations, 2.3×10^{-6} cm^{-1}, is adopted as a conservative estimate for the uncertainty of the magic number. In addition, 11 artificial transitions were used to link the largest floating components to the PCs. These transitions form bridges between the principal components and the floating components of disconnected higher-J transitions. In fact, these transitions link the ground state to series of states with $K_a = 8$, $K_a = 10$, and $K_a = 11$. The values of these artificial transitions are taken from the effective Hamiltonian study of 88NaReDaJo [87].

First-principles computations are capable of estimating small energy splittings very accurately [122]; thus, we decided to add the $J_{J,0/1}$ separations as virtual lines to the dataset. They are part of a source tagged as '21virt' (see Table 3). These virtual transitions are distributed into four segments, based on the magnitude of the splittings and thus on their assumed uncertainties. Through these virtual lines 199 further rovibrational energy levels could be determined: the experimentally unavailable states of certain $J_{J,0/1}$ pairs.

Table 3: Data source segments and their characteristics for the $H_2{}^{12}C^{16}O$ molecule[a]

Segment tag	Range	$A/N/V$	ESU	MSU	LSU	Recalib. Factor
72TuToTh [61]	0.483 28–0.483 28	1/1/1	2.67e-09	2.67e-09	2.67e-09	
71TuToTh [58]	0.141 30–0.165 74	3/3/3	3.67e-09	3.67e-09	5.34e-09	
81ChMi [77]	0.002 373–0.064 793	14/9/9	6.67e-09	1.00e-08	3.34e-08	
73ChGu [62]	0.000 003–0.966 50	23/21/21	1.00e-08	1.00e-08	3.66e-07	
73ChGu_S2 [62]	2.415 3–2.415 3	1/1/1	3.34e-05	3.34e-05	3.34e-05	
68Takami [53]	0.000 022–0.001 829	12/10/10	1.67e-08	3.15e-08	6.44e-07	
77ChGu [70]	0.000 005–0.002 305	39/39/35	3.34e-08	3.34e-08	1.33e-07	
96BoDePoLi [85]	0.000 003–0.708 93	68/35/35	3.34e-08	1.67e-07	1.67e-07	
96BoDePoLi_S2 [85]	0.000 059–46.275	93/45/44	1.00e-06	1.00e-06	4.37e-06	
96BoDePoLi_S3 [85]	0.165 27–63.241	91/72/72	3.34e-06	3.34e-06	1.67e-05	
96BoDePoLi_S4 [85]	34.009–84.711	21/21/21	1.67e-04	1.67e-04	1.67e-04	
21AlTeYuMe	9.390 7–10.035	7/7/7	7.00e-08	7.00e-08	1.33e-07	
21AlTeYuMe_S2	8.237 6–12.988	82/82/82	7.00e-07	7.00e-07	4.74e-06	
66TaEvSh [147]	0.000 153–0.000 610	2/2/2	1.00e-07	1.00e-07	1.33e-07	
77FaKrMu [71]	0.002 373–0.082 838	4/4/4	1.67e-07	1.67e-07	1.67e-07	
63Esterowi [50]	0.010 044–0.035 553	4/4/4	2.50e-07	4.17e-06	1.11e-05	
80CoWi [76]	0.000 003–15.039	127/95/94	3.34e-07	3.34e-07	3.15e-06	
17MuLe [106]	45.744–49.915	45/45/45	3.34e-07	3.34e-07	3.34e-07	
88NaReDaJo [87]	0.000 020–0.561 82	10/10/10	6.67e-07	6.67e-07	1.12e-05	
88NaReDaJo_S2 [87]	0.000 005–10.029	64/64/63	1.00e-06	1.00e-06	1.72e-05	
88NaReDaJo_S3 [87]	608.85–630.67	2/2/2	5.00e-05	1.00e-05	1.00e-05	
88NaReDaJo_S4 [87]	922.63–1 578.4	314 9/312 8/312 8	2.00e-04	1.19e-04	2.01e-02	
88NaReDaJo_S5 [87]	681.57–1 201.9	9/9/9	5.00e-03	1.00e-03	1.00e-03	
03ThCaRiMu [86]	0.163 02–0.164 96	3/3/2	8.34e-07	8.34e-07	1.00e-06	
03BrMuLeWi [91]	27.793–66.778	136/136/136	1.00e-06	1.00e-06	2.74e-05	
09MaPeJaBa [100]	5.016 8–30.115	172/172/171	1.00e-06	1.00e-06	1.33e-05	
12ElCuGuHi [104]	23.353–58.596	87/87/87	1.00e-06	1.00e-06	5.55e-06	
21virt	0.000 000–0.000 000	446/446/446	1.00e-06	1.00e-06	1.00e-06	
21virt_S2	0.000 001–0.000 009	178/177/177	1.00e-05	1.00e-05	2.21e-04	
21virt_S3	0.000 010–0.000 098	157/151/151	1.00e-04	1.00e-04	2.78e-03	
21virt_S4	0.000 100–0.000 999	168/166/166	1.00e-03	1.00e-03	3.89e-03	
72Nerf [60]	1.610 6–10.035	15/15/15	1.47e-06	1.60e-06	7.86e-06	
51LaSt [45]	0.245 59–2.429 6	18/18/18	1.67e-06	2.40e-06	2.03e-05	
56Erlandss [148]	2.429 6–7.528 5	9/8/8	1.67e-06	1.60e-05	2.79e-05	
64OkTaMo [52]	0.000 153–2.437 1	70/49/44	1.67e-06	1.80e-06	2.66e-05	
97CaHaDe [146]	10.539–10.539	1/1/1	2.30e-06	2.30e-06	2.30e-06	
72JoLoKi [59]	0.000 153–4.504 1	37/10/10	3.34e-06	8.34e-07	5.00e-06	
78DaWiBe [72]	0.353 87–12.187	86/82/82	6.67e-06	6.67e-06	2.31e-05	
73ChFrJoOk [63]	0.553 19–1.979 8	7/7/7	1.67e-05	1.67e-05	2.67e-05	
85TiChKuHu [80]	4 211.6–5 224.0	100 5/100 5/100 3	1.00e-04	1.10e-04	1.16e-02	
82BrJoMcWo [79]	1 693.1–1 793.4	248/248/248	4.00e-04	1.59e-04	8.99e-04	
79BrHuPi [74]	2 700.0–3 000.2	319 3/318 9/318 3	5.00e-04	3.27e-04	4.52e-02	
81SwSa [78]	1 707.1–1 746.9	76/76/76	5.00e-04	6.50e-04	3.38e-03	
88ClVa [82]	2 867.2–2 880.4	24/22/22	5.00e-04	3.48e-04	7.23e-03	
94ItNaTa [84]	2 276.2–2 553.6	320/320/317	5.00e-04	3.91e-04	5.56e-03	
10JaLaTcGa [103]	1 675.0–3 089.8	782/781/781	5.00e-04	1.62e-04	6.45e-03	1.000 001 293
07TcPeLa_S2 [97]	0.000 006–10.029	84/84/84	2.10e-04	1.00e-04	2.25e-03	
07TcPeLa [97]	927.68–1 821.6	402 4/110 1/110 1	8.00e-04	1.04e-04	5.00e-03	

Continued on next page

Table 3 – *Continued from previous page*

Segment tag	Range	$A/N/V$	ESU	MSU	LSU	Recalib. Factor
06PeBrUtHa [96]	2 756.6–2 864.6	147/143/143	1.00e-03	1.00e-03	3.82e-02	
09CiMaCi [102]	4 350.9–4 360.6	49/46/36	1.00e-03	1.00e-03	7.97e-03	
07SaBaHaRi [99]	5 597.8–5 698.3	424/422/418	1.50e-03	1.00e-03	9.08e-03	
17TaAdNg [107]	3 398.7–3 529.7	786/786/785	1.60e-03	1.11e-03	3.66e-02	
73Toth [65]	3 428.2–3 507.4	299/299/298	3.00e-03	2.83e-03	4.23e-02	
77AlJoMc [68]	945.23–1 540.0	991/922/904	5.00e-03	3.94e-03	4.57e-02	
77AlJoMcb [69]	1 483.0–1 518.1	70/70/70	5.00e-03	4.14e-03	3.57e-02	
76NaYaKu [149]	2 643.9–3 011.8	184 8/184 5/171 1	3.00e-02	1.68e-02	9.89e-02	

[a] Tags denote segments used in this study. The column 'Range' indicates the range (in cm^{-1}) corresponding to validated wavenumbers within the transition list. A is the number of assigned transitions, N is the number of non-redundant lines (with distinct wavenumbers or labels), and V is the number of validated transitions obtained at the end of the xMARVEL analysis. In the heading of this table, ESU, MSU, and LSU denote the estimated, the median, and the largest segment uncertainties, respectively, in cm^{-1}. Rows are arranged in the order of the ESUs with the restriction that the segments of the same data source should be listed consecutively.

3. The rovibrational database

3.1. Overview

Tables 3 and 4 present an overview of the experimental information considered during this project. Each experimental source is given a tag composed of the last two digits of the year of publication and letters of the names of up to the first four co-authors.

Table 4: High-resolution spectroscopic studies on $H_2{}^{12}C^{16}O$ which were considered but not utilized during the present MARVEL analysis, with reason for the exclusion.

Tag	Range / cm^{-1}	Reason for exclusion
17FjHeBaLe [28]	6230 – 6240	700 K emission spectrum, line parameters not provided
15RuHeHeFi [105]	6547 – 7051	No line assignments
09PeJaTcLa [101]	1600 – 3200	Calculated line positions only
07ZhGaDeHu [98]	6351 – 6362	No line assignments
06FlLaSaSh [94]	3096 – 5263	Data not made available by the authors
06PeVaDa [95]	2600 – 3100	No line parameters provided, data not made available by the authors
05StGaVeRu [93]	6547 – 6804	No line assignments
03PeKeFl [92]	1000 – 2000	Data not made available by the authors
02BaCoHaPe [90]	5600 – 5700	Data analysed by 07SaBaHaRi [99]
96BoHaGrSt [88]	–	Dispersed fluorescence, vibrational state data only
96LuCoFrCr [89]	7800 – 15200	No line parameters provided
89ReNaDaJo [83]	890 – 1590	No line parameters provided
87NaDaRe [81]	1148 – 1193	Lines included in 88NaReDaJo [87]
78Pine [73]	2700 – 3000	No line parameters provided
75Nerf [66]	1 – 10	Lines are given in 72Nerf [60]
73JoMc [64]	1707 – 1767	No line parameters provided
70TuThTo [56]	0.15 – 0.15	Line is given in 71TuToTh [58]
60OkHiSh [48]	0.98	Lines are given in 64OkTaMo [52]

Table 3 summarizes the sources included in our final MARVEL analysis and gives statistical information about the transitions these sources contain. We utilized data from 43 literature sources, including this work, yielding 19 831 transitions, of which 16 596 are non-redundant.

Table 4 lists sources that were *not* included in the final analysis. A number of other older sources [47, 51, 55] were also excluded from the present analysis, as their measurements have been superseded by those of significantly more accurate studies.

3.2. Source-specific comments

A significant problem we faced during the data collection was that there are several publications [92, 94, 95] for $H_2{}^{12}C^{16}O$ where the authors did not provide the direct measured data in their original paper and when approached they turned down our request to send the measured data forming the basis of their existing publication. Similar problems, and related issues, have been highlighted in a recent paper by Gordon *et al.* [150]. Seemingly it is not straightforward to include old data into new data compilations.

Another significant issue is that a number of sources do not provide a clear statement about the uncertainties of the observed lines. Thus, we had to estimate them by various means, which included comparisons with other sources as well as combination-difference relations. Such sources include 76NaYaKu [149], 82BrJoMcWo [79], 88ClVa [82], 85TiChKuHu [80], 77AlJoMc [68], 77AlJoMcb [69], and 10JaLaTcGa [103]. Since the authors of 10JaLaTcGa [103] state that their line positions were not calibrated, we used an xMARVEL facility to calibrate the wavenumbers of the measured transitions published in 10JaLaTcGa. This gave a calibration factor of 1.000 001 148 for this source.

64OkTaMo [52] provides high-resolution pure rotational transitions between levels in vibrationally excited states. However, 78DaWiBe [72] found it necessary to reassign the vibrational states in this source; we have adopted and in fact validated the assignments of 78DaWiBe.

76NaYaKu [149] is an older and relatively low-resolution source, which nonetheless contains lines for which no data are available from alternative sources. The authors used a compact, non-standard notation for the assignments, which had to be unpicked. A total of 134 lines could not be validated and thus were removed. Transitions involving high K_a states did not resolve the K-doublets, *i.e.*, the K_c quantum number. For these transitions we used two lines corresponding to both possible transitions.

88NaReDaJo [87] gives only calculated line positions and residuals; thus, the observed frequencies were reconstructed from this information. Similarly, the tables in 79BrHuPi [74] are of very poor quality and their line frequency data could only be accurately reconstructed by extensive comparison with HITRAN [151]; 88ClVa [82] also provides a small portion of 79BrHuPi's spectrum in readable form.

02BaCoHaPe [90] recorded a spectrum of the $5\nu_2$ overtone; this spectrum was analyzed by 07SaBaHaRi [99], who also provided the data (C.M. Western, private communication, 2020). These

studies did not contain an estimated uncertainty; thus, an estimated value of 0.0015 cm^{-1} was adopted on the basis of combination difference relations.

72JoLoKi [59] presents an extensive compilation of early microwave experiments on formaldehyde. Although this is a secondary source, some data were taken from here as the primary sources are not available to us. 72JoLoKi also contains tabulations of hyperfine-resolved transitions for the $1_{01}-1_{11}$, $2_{11}-2_{12}$, and $3_{12}-3_{13}$ rotational lines. Other microwave studies, including 59TaShSh [46], 70TuThTo [56], 71TuToTh [58], 72TuToTh [61], and 17MuLe [106] also present hyperfine-resolved data. Within the present study we completely neglect hyperfine effects and, where necessary, use central, hyperfine-unresolved line positions.

4. Results and Discussion

4.1. Validation

According to Table 3, we considered for validation 16 596 non-redundant transitions measured for $H_2{}^{12}C^{16}O$. 13 of these transitions are artificial (see above) and 143 do not attach to the principal components, they remain parts of floating components. The transitions of the giant components of the SN of $H_2{}^{12}C^{16}O$ were validated using several techniques.

193 transitions, including a few which did not obey the selection rules governing electric-dipole-allowed transitions, were removed at the first stage of validation. In almost all cases these transitions were ones for which alternative, validated wavenumber entries were available from other sources. The number of validated transitions within each segment is given in Table 3. The transitions which could not be validated are retained in the transitions list given in the supplementary data, but they are given there as a negative wavenumber entry, which means that they are ignored during the processing of the data by xMARVEL. Therefore, these transitions do not contribute to the final empirical energy levels.

The other important step in the validation process involved comparisons with the AYTY line list [113]. These comparisons were performed iteratively between the empirical (xMARVEL) and the AYTY energy levels. During the first phase, the comparisons identified a number of issues with the original xMARVEL dataset in the form of incorrect quantum numbers or scanning errors. Once these were corrected, only a few lines were found for which the upper states had no reasonable match within the AYTY list. These transitions are augmented with a comment 'theoretical mismatch' in the MARVEL XML file given in the supplementary material. Those excluded lines which violate the electric-dipole selection rules have the comment 'wrong labels' in the XML file. At the end, we were able to validate 16 403 of the collected transitions.

4.2. Final energies

The MARVEL analysis yielded, in total, 5029 validated empirical rovibrational energies for $H_2{}^{12}C^{16}O$; they are provided in the supplementary material. The highest rotational quantum num-

Table 5: MARVEL-based vibrational band origins (VBO) of $H_2{}^{12}C^{16}O$ and their literature counterparts obtained from accurate effective Hamiltonian fits.[a]

Band	Symmetry	VBO(MARVEL)	N_0	$N_{\rm RL}$	$J_{\rm max}$	VBO(lit)
ν_0	a_1	0.0	31	525	38	0.0
ν_4	b_1	1167.256 76(10)	6	346	30	1167.258(2) [68]
						1167.256 28(2) [92]
ν_6	b_2	1249.094 42(10)	3	405	30	1249.091(2) [68]
						1249.094 68(2) [92]
ν_3	a_1	1500.174 50(10)	4	382	30	1500.176(3) [68]
						1500.174 74(12) [92]
ν_2	a_1	1746.009 14(10)	4	446	37	1746.008 9(1) [79]
						1746.008 86(13) [92]
$2\nu_4$	a_1	–	0	65	11	2327.523 9(5) [95]
						2327.1(8) [75]
$\nu_4+\nu_6$	a_2	–	0	47	11	2422.970 1(50) [95]
$2\nu_6$	a_1	–	0	81	25	2494.354 3(5) [95]
$\nu_3+\nu_4$	b_1	–	0	15	10	2667.048 1(20) [95]
						2655.5 [74]
$\nu_3+\nu_6$	b_2	2719.156 04(50)	1	232	25	2719.155 9(10) [74]
ν_1	a_1	2782.456 91(50)	2	440	36	2782.456 9(10) [74]
ν_5	b_2	2843.323 54(12)	4	388	35	2843.325 6(10) [74]
$\nu_2+\nu_4$	b_1	–	0	153	24	2905.968 5(20) [95]
						2905(1) [74]
$2\nu_3$	a_1	–	0	38	25	2998.987 3(5) [95]
						2999.5(5) [74]
$\nu_2+\nu_6$	b_2	3000.065 74(50)	1	100	21	3000.065 6(10) [74]
$2\nu_2$	a_1	3471.720 8(78)	2	373	31	3471.718(4) [65]
$\nu_1+\nu_4$	b_1	3941.530 8(10)	1	30	10	–
$\nu_4+\nu_5$	b_2	3996.518 6(10)	1	35	9	–
$\nu_3+\nu_5$	b_2	4335.0989 4(10)	1	170	24	–
$2\nu_2+\nu_6$	b_2	–	0	207	26	4734.207 8(50) [94]
$3\nu_2$	a_1	–	0	176	26	5177.759 52(70) [94]
$2\nu_5$	a_1	5651.196 4(15)	1	179	20	–

[a]The VBO values are in cm^{-1}. The uncertainties of the last VBO digits are given in parentheses. The symmetry of the band, the number of transitions determining a particular VBO (N_0), as well as the number of rotational levels ($N_{\rm RL}$) and the maximum J value within a given vibrational band are also displayed.

ber is $J_{\rm max}=38$ and the empirical energies go up to 6188 cm^{-1}; there are transitions which probe energy levels higher than this but none of them are assigned. Thus, all empirical energy levels are well below the minima corresponding to hydroxymethylene. A large number of further experimental studies are needed to reach that dynamically important and interesting region. The region covered is also considerably more limited than that covered by SEP measurements in the 1980s [10].

Table 5 presents the vibrational band origins (VBO) and a summary of the number of empirical rovibrational energy levels determined for each vibrational state. The bands $2\nu_3+\nu_6$, $\nu_2+\nu_5$, and $\nu_2+\nu_3+\nu_4$, which have a combined total of only 6 levels, have been omitted from the table. Table 5 also gives term values of this and previous studies, *i.e.*, levels with $J=0$ for given vibrational bands.

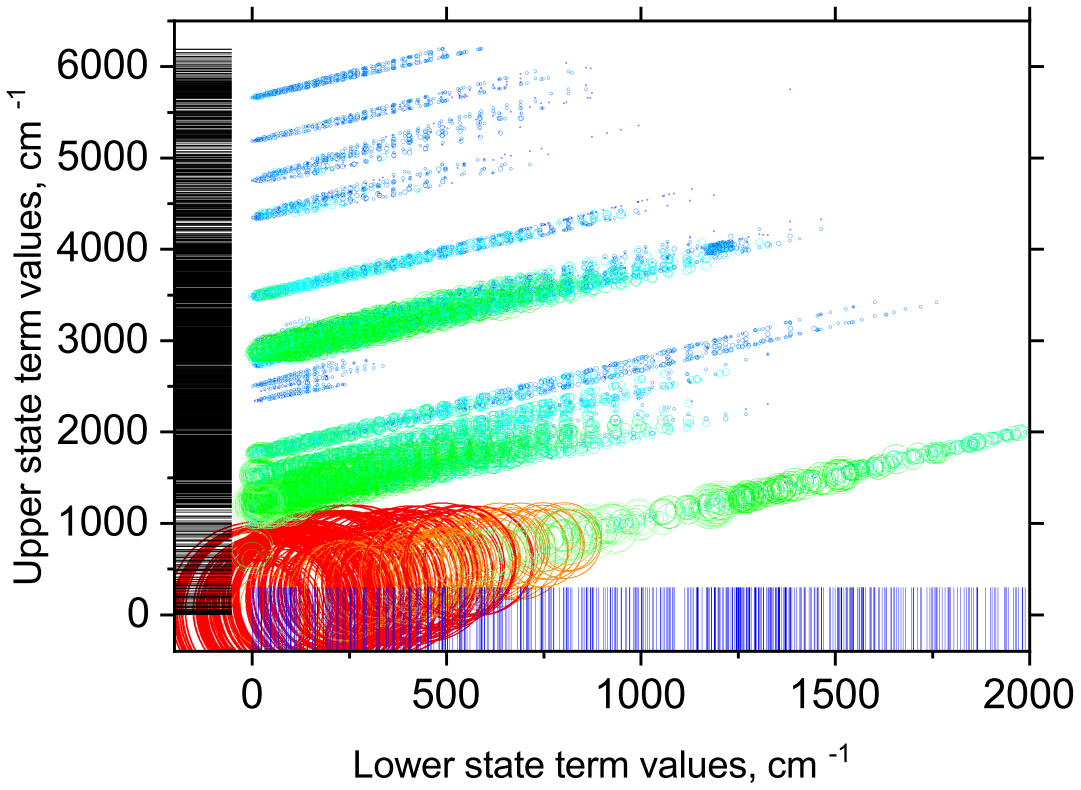

Figure 2: The upper-state energies of the experimental transitions used in this work, against corresponding lower-state energies of $H_2{}^{12}C^{16}O$. The vertical bars along the horizontal axis show the lower state energies, while the horizontal bars along the vertical axis give the upper state energies. Each circle represents a particular transition, with the size proportional to the number of transitions supporting the corresponding upper state. This value ranges from 1 (dark blue) to 102 (red).

Table 5 contains term values for 14 vibrational band origins, including the six fundamentals, determined during this study. The term values of the ν_2, ν_3, and ν_4 fundamentals are determined particularly accurately, in part because in these cases the upper states have been subjected to high-accuracy microwave studies; indeed, such studies for ν_3 and ν_4 form part of the present work. We note that these fundamentals are all characterized by at least three transitions. In contrast, the term values of the combination bands are much less accurate and determined by only one, or in one case two, transitions. It is important to note that the fundamentals of Ref. [68] result from effective-Hamiltonian calculations, which may yield higher apparent accuracy than the present MARVEL treatment.

Figure 2 provides a visual representation of the spectroscopic network of $H_2{}^{12}C^{16}O$, showing the upper-state energies of the measured transitions against corresponding lower-state energies, and giving a visual impression of the number of transitions linking them.

Table 6: Pure rotational frequencies of $H_2{}^{12}C^{16}O$ lines under protection by the National Academies of Sciences, Engineering, and Medicine (NASEM) [152] and their various experimental and empirical determinations. The uncertainties of the last few frequency digits are indicated in parentheses.

$f_{\rm NASEM}$/GHz	Line assignment	$f_{\rm MARVEL}$/GHz	$f_{\rm expt}$/GHz
4.829 66	$\nu_0, 1_{1,0} \leftarrow 1_{1,1}$	4.829 659 960(50)	4.829 659 960(50) [58]
			4.829 660 0(10) [85]
			4.829 649 0(50) [62]
			4.829 660(10) [59]
14.488	$\nu_0, 2_{1,1} \leftarrow 2_{1,2}$	14.488 478 810(80)	14.488 478 810(80) [61]
			14.488 479 0(10) [85]
			14.488 650(20) [52]
			14.488 650(50) [45]
			14.488 65(10) [62]
140.84	$\nu_0, 2_{1,2} \leftarrow 1_{1,1}$	140.839 502(10)	140.839 502(10) [85]
			140.839 526(32) [60]
			140.839 300(50) [148]
145.603	$\nu_0, 2_{02} \leftarrow 1_{0,1}$	145.602 949(10)	145.602 949(10) [85]
			145.602 966(34) [60]
			145.603 100(50) [148]
150.498	$\nu_0, 2_{1,1} \leftarrow 1_{1,0}$	150.498 334(10)	150.498 334(10) [85]
			150.498 355(34) [60]
			150.498 200(50) [148]
218.222	$\nu_0, 3_{0,3} \leftarrow 2_{0,3}$	218.222 192(10)	218.222 192(10) [85]
			218.222 186(49) [60]
			218.221 600(50) [148]

4.3. Protected formaldehyde lines

The National Academies of Sciences, Engineering, and Medicine (NASEM) maintains a list of key long-wavelength transitions relevant for astrophysical studies [152]. This list contains six transitions belonging to $H_2{}^{12}C^{16}O$; they are given in Table 6. Some previous MARVEL studies, notably on water [110, 120] and ammonia [138], allowed the accuracy, to which some of these lines were known, to be improved using MARVEL. In the case of $H_2{}^{12}C^{16}O$, however, we find that the uncertainties in our MARVEL-determined frequencies simply match those of the current best laboratory determinations; for a discussion how these uncertainties are determined, see Ref. [110]. Nevertheless, Table 6 is still useful as it shows all highly-accurate studies of the NASEM-protected lines.

5. Updated AYTY line list

The AYTY line list [113] of $H_2{}^{12}C^{16}O$ contains approximately 10 billion transitions linking 10.3 million rotational-vibrational states. These states are those with $J \leq 70$ which lie up to 10 000 cm^{-1} above the ground state. As part of this study, we replace those energy levels of the AYTY list which are determined empirically by the MARVEL process.

Table 7: Extract from the H_2CO state file. The full table is available from `www.exomol.com`.[a]

I	$\tilde{E}$/cm^{-1}	g	J	δ/cm^{-1}	τ/s	$\Gamma_{\rm tot}$	v_1	v_2	v_3	v_4	v_5	v_6	$\Gamma_{\rm vib}$	K_a	K_c	$\lvert C_i^2\rvert$	n_1	n_2	n_3	n_4	n_5	n_6	K	$\tilde{E}_{\rm AYTY}$/cm^{-1}
1	0.000000	1	0	0.000001	Inf	A1	0	0	0	0	0	0	A1	0	0	1.00	0	0	0	0	0	0	Ma	0.000000
2	1500.174503	1	0	0.000100	3.1423E-01	A1	0	0	1	0	0	0	A1	0	0	1.00	0	0	0	0	1	0	Ma	1500.120955
3	1746.009136	1	0	0.000100	3.1935E-02	A1	0	1	0	0	0	0	A1	0	0	1.00	1	0	0	0	0	0	Ma	1746.045388
4	2327.497142	1	0	0.200000	4.7496E-01	A1	0	0	0	2	0	0	A1	0	0	1.00	0	0	0	0	0	2	Ca	2327.497142
5	2494.322937	1	0	0.200000	2.0931E-01	A1	0	0	0	0	0	2	A1	0	0	1.00	0	0	0	1	1	0	Ca	2494.322937
6	2782.456913	1	0	0.000500	1.5673E-02	A1	1	0	0	0	0	0	A1	0	0	1.00	0	0	1	0	0	0	Ma	2782.410921
7	2999.006647	1	0	0.200000	1.0513E-01	A1	0	0	0	0	0	2	A1	0	0	1.00	0	0	0	1	1	0	Ca	2999.006647
8	3238.937891	1	0	0.200000	2.9533E-02	A1	0	1	1	0	0	0	A1	0	0	1.00	1	0	0	0	1	0	Ca	3238.937891
9	3471.720843	1	0	0.007770	1.5448E-02	A1	0	2	0	0	0	0	A1	0	0	1.00	2	0	0	0	0	0	Ma	3471.719306
10	3825.967015	1	0	0.300000	1.6623E-01	A1	0	0	1	2	0	0	A1	0	0	1.00	0	0	0	0	1	2	Ca	3825.967015
11	3936.435541	1	0	0.300000	3.3267E-02	A1	0	0	3	0	0	0	A1	0	0	1.00	0	0	0	3	0	0	Ca	3936.435541
12	4058.101422	1	0	0.300000	3.0046E-02	A1	0	1	0	2	0	0	A1	0	0	1.00	1	0	0	0	0	2	Ca	4058.101422

[a] I: state identifier; $\tilde{E}$: state term value; g: state degeneracy; J: state rotational quantum number; δ: energy uncertainty; τ: lifetime; $\Gamma_{\rm tot}$: total symmetry in $C_{2\nu}(M)$; $v_1 - v_6$: normal mode vibrational quantum numbers; $\Gamma_{\rm vib}$: symmetry of vibrational contribution in $C_{2\nu}(M)$; K_a and K_c: rotational quantum numbers; $|C_i^2|$: largest coefficient used in the assignment; $n_1 - n_6$: TROVE vibrational quantum numbers; K: data kind indicating if the term value is based on the MARVEL ('Ma') or the AYTY energy list ('Ca'); $\tilde{E}_{\rm AYTY}$: original AYTY state term value.

The rovibrational states were matched on the basis of quantum numbers and then checked using the energies. As a result, 367 779 transition frequencies are determined using the empirical energy levels of this study. Of these, 183 673 lie above the dynamic HITRAN intensity cutoff [153]. These numbers should be compared to the 16 596 non-redundant transitions which form the input to the original spectroscopic network of $H_2{}^{12}C^{16}O$. It can be seen that this process leads to a significant increase in the number of transitions whose line centres are determined to high-resolution experimental accuracy.

Obviously, 5029 empirically determined energy levels is only a small portion of the 10.3 million entries in the original AYTY line list. We therefore had to estimate the (significantly larger) uncertainties associated with the calculated energy levels. This is important, not least because it allows transitions that are predicted with high accuracy to be easily identified. We estimated the uncertainties, in cm^{-1}, of the computed levels using the formula

$$\delta = 0.1\,(v_1 + v_2 + v_3 + v_4 + v_5 + v_6) + 0.005J(J+1).$$

This update is in line with the requirements of the 2020 release of ExoMol [154] and is designed to facilitate the use of the data in high-resolution studies by quantifying the uncertainty associated with each transition and hence identifying those known with the required accuracy for a given study.

Table 7 gives a small portion of the updated ExoMol States file in standard ExoMol format [155, 154]. The complete file along with the AYTY Trans file, which is unchanged by the current procedure, can be obtained from the ExoMol website (`www.exomol.com`).

The HITRAN database [151] contains limited data on $H_2{}^{12}C^{16}O$: besides pure rotations it covers

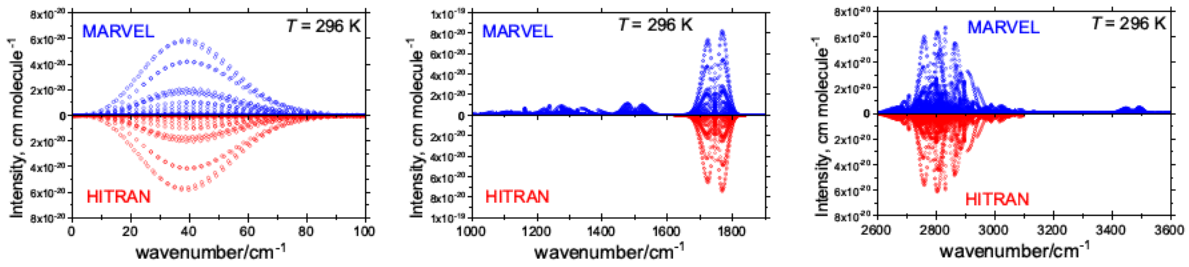

Figure 3: Room-temperature (T = 296 K) spectra of $H_2{}^{12}C^{16}O$ in three different regions covered by HITRAN 2016 [151]. The upper panels, in blue, show stick spectra simulated using the MARVEL energy term values from this work and the Einstein-A coefficients from the AYTY line. The lower panels, in red, show the corresponding spectra taken from HITRAN 2016.

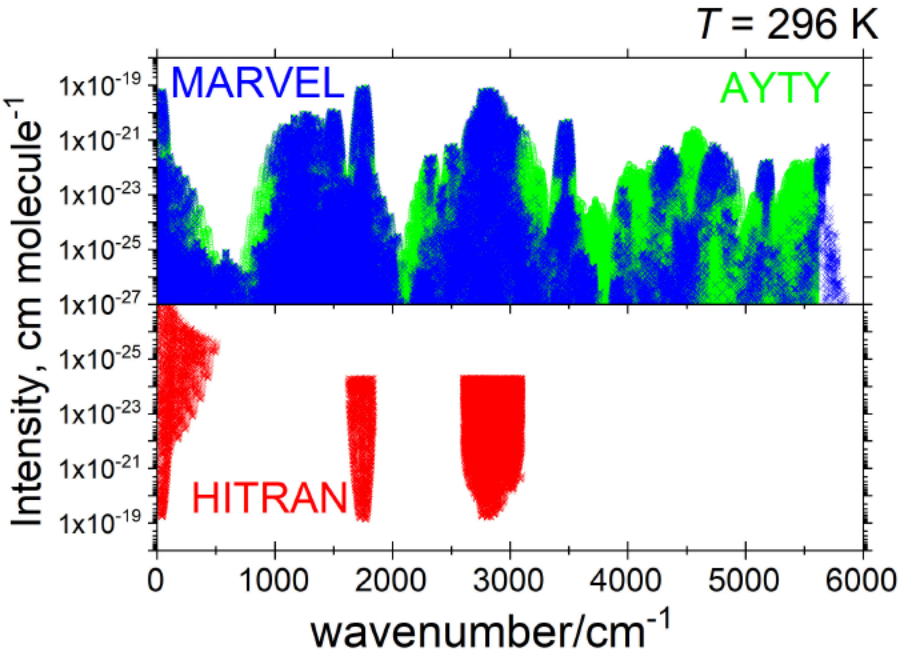

Figure 4: Room temperature (T = 296 K) spectra of $H_2{}^{12}C^{16}O$ from three different sources: lower panel, HITRAN 2016 [151]; upper panel, this work (see caption of Fig. 3) where possible or else from the AYTY [113] line list.

only two bands. Figure 3 gives a comparison for these regions. The agreement is very good and shows that our MARVEL analysis is largely sufficient to cover these regions. Figure 4 illustrates the relative (in)completeness of the HITRAN and our MARVEL data sets when used to simulate the room temperature spectra of $H_2{}^{12}C^{16}O$. There are a number of missing bands in HITRAN and the database can now be supplemented with our synthetic line list constructed using the line positions determined to experimental accuracy using MARVEL and AYTY transition intensities.

The AYTY line list was actually designed for treating formaldehyde in hot environments. In order to illustrate the lack of experimental data at high temperatures, Fig. 5 shows T = 1000 K absorption spectra simulated with the same three source as above: MARVEL line positions (this

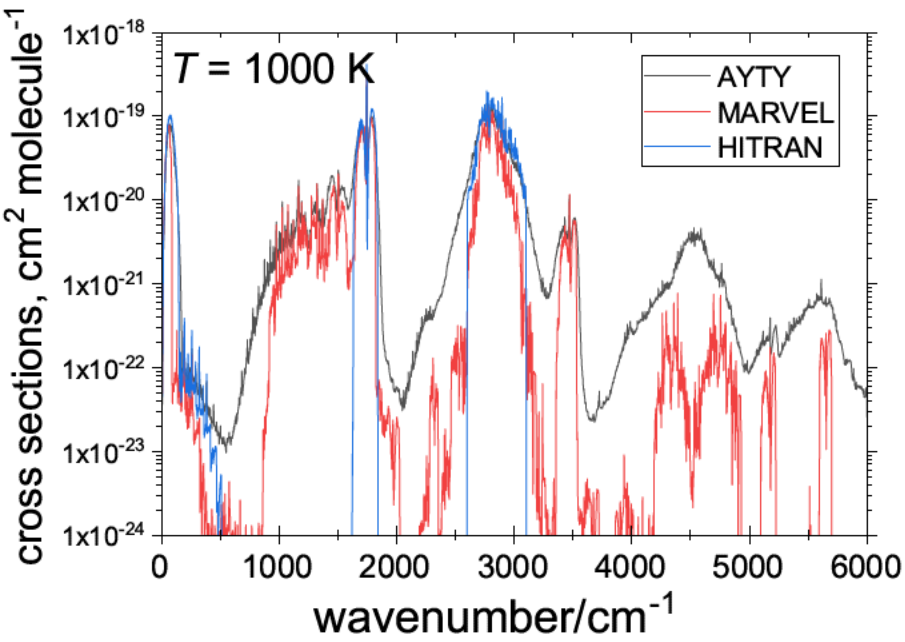

Figure 5: High temperature (T = 1000 K) spectra of $H_2{}^{12}C^{16}O$ from three different sources: HITRAN 2016 [151], AYTY [113], and this work (see also caption to Fig. 3).

work) combined with the AYTY Einstein-A coefficients, the HITRAN line list, and the AYTY line list. It is clear that at high temperatures only AYTY provides the spectroscopic coverage required for high temperatures and that known laboratory spectra are not capable of giving a complete representation of hot formaldehyde.

6. Summary and Conclusions

Apart from a few sources where the authors were reluctant to provide their published results for analysis [92, 94, 95], all literature lines measured for $H_2{}^{12}C^{16}O$ have been collected and analyzed during this study. The information contained in the literature sources was augmented by new measurements results, including seven Lamb-dip lines and 82 further lines, all corresponding to rotational transitions within the ground, ν_3, ν_4, and ν_6 vibrational states. The analysis utilized the Measured Active Rotational-Vibration Levels (MARVEL) approach and the xMARVEL code. A characteristic of MARVEL is that it is an "active" approach, which means that should new sources, or even existing sources that have not been included, became available it is straightforward to include them in a renewed analysis and produce an updated version of the line-by-line database assembled for $H_2{}^{12}C^{16}O$.

Of the total of 19 831 transitions processed, which come from 43 sources including this work, 16 403 could be validated, providing 5029 empirical energy levels of $H_2{}^{12}C^{16}O$ with statistically well-defined uncertainties. Our newly-determined empirical rotational-vibrational energy levels are

used to improve the accuracy of ExoMol's AYTY line list for hot formaldehyde [113]. This improved line list is available as supplementary material, along with the xMARVEL files, containing all the rovibrational transitions collated, whether validated or not, as well as all the empirical energy levels derived during this study.

It is the stated plan of the ExoMol project [112] to update all ExoMol line lists to include both empirical energy levels, where available, and uncertainties for all the energy levels; thus allowing the uncertainty associated with any transition to be estimated. These data will become a standard part of the ExoMol line list and also form input for the new ExoMolHR database, which provides data only on lines of higher intensity whose wavelengths are known to high accuracy. So far only a limited number of ExoMol line lists are available with specified uncertainties in the energy levels. These include important line lists for which MARVEL data were already available, namely those for water [156], AlH [157], $^{12}C_2$ [131], $^{12}C_2H_2$ [158] and $^{48}Ti^{16}O$ [158], and recently produced line lists including those for CO_2 [159], H_3O^+ [160] and NH_3 [161]. The present study is the first in a series where a MARVEL analysis is performed with the intention of updating an available line list.

Acknowledgments

We thank Dr. Colin Western for providing the data generated by 07SaBaHaRi [99]. The work at UCL is supported by STFC Projects No. ST/M001334/1 and ST/R000476/1, and the European Research Council (ERC) under the European Union's Horizon 2020 research and innovation programme through Advance Grant number 883830. The work performed in Budapest received support from NKFIH (grant no. K119658), from the grant VEKOP-2.3.2-16-2017-000, and from the ELTE Institutional Excellence Program (TKP2020-IKA-05) financed by the Hungarian Ministry of Human Capacities. The work performed in Bologna was supported by the Università di Bologna (RFO funds) and by MIUR (Project PRIN 2015: STARS in the CAOS, Grant Number 2015F59J3R).

References

[1] J. K. McLaughlin, Formaldehyde and cancer: a critical review, Int. Arch. Occ. Env. Hea. 66 (1994) 295–301.

[2] G. D. Nielsen, P. Wolkoff, Cancer effects of formaldehyde: a proposal for an indoor air guideline value, Arch. Toxicol. 84 (2010) 423–446.

[3] Q. He, J. Li, Q. Feng, Ppb-level formaldehyde detection system based on a 3.6 μm interband cascade laser and mode-locked cavity enhanced absorption spectroscopy with self-calibration of the locking frequency, Infrared Phys. Techn. 105 (2020) 103205.

[4] D. C. Moule, A. D. Walsh, Ultraviolet spectra and excited states of formaldehyde, Chem. Rev. 75 (1975) 67–84.

[5] D. J. Clouthier, D. A. Ramsay, The spectroscopy of formaldehyde and thioformaldehyde, Annu. Rev. Phys. Chem. 34 (1983) 31–58.

[6] C. B. Moore, J. C. Weisshaar, Formaldehyde photochemistry, Annu. Rev. Phys. Chem. 34 (1983) 525–555.

[7] R. P. Wayne, Chemistry of atmospheres, Oxford University Press, New York, 2000.

[8] D. Townsend, S. A. Lahankar, S. K. Lee, S. D. Chambreau, A. G. Suits, X. Zhang, J. Rheinecker, L. B. Harding, J. M. Bowman, The roaming atom: straying from the reaction path in formaldehyde decomposition, Science 306 (2004) 1158—1161.

[9] P. Zhang, S. Maeda, K. Morokuma, B. J. Braams, Photochemical reactions of the low-lying excited states of formaldehyde: T_1/S_0 intersystem crossings, characteristics of the S_1 and T_1 potential energy surfaces, and a global T_1 potential energy surface, J. Chem. Phys. 130 (2009) 114304.

[10] D. E. Reisner, R. W. Field, J. L. Kinsey, H.-L. Dai, Stimulated emission spectroscopy: a complete set of vibrational constants for $\tilde{\mathrm{X}}\,^1A_1$ formaldehyde, J. Chem. Phys. 80 (1984) 5968–5978.

[11] A. G. Császár, Anharmonic molecular force fields, WIREs Comput. Mol. Sci. 2 (2012) 273–289.

[12] J. M. L. Martin, T. J. Lee, P. R. Taylor, An accurate *ab initio* quartic force-field for formaldehyde and its isotopomers, J. Mol. Spectrosc. 160 (1993) 105–116.

[13] S. Carter, N. Pinnavaia, N. C. Handy, The vibrations of formaldehyde, Chem. Phys. Lett. 240 (1995) 400–408.

[14] D. C. Burleigh, A. B. McCoy, E. L. Sibert, An accurate quartic force field for formaldehyde, J. Chem. Phys. 104 (1996) 480–487.

[15] W. J. Morgan, D. A. Matthews, M. Ringholm, J. Agarwal, J. Z. Gong, K. Ruud, W. D. Allen, J. F. Stanton, H. F. Schaefer, Geometric energy derivatives at the complete basis set limit: application to the equilibrium structure and molecular force field of formaldehyde, J. Chem. Phys. 14 (2018) 1333–1350.

[16] P. Jensen, P. Bunker, The geometry and the inversion potential function of formaldehyde in the $\mathrm{A}\,^1A_2$ and a^3A_2 electronic states, J. Mol. Spectrosc. 94 (1982) 114–125.

[17] J. D. Goddard, Y. Yamaguchi, H. F. Schaefer, Features of the H_2CO potential energy hypersurface pertinent to formaldehyde photodissociation, J. Chem. Phys. 75 (1981) 3459–3465.

[18] A. F. Jalbout, C. M. Chang, The H_2CO potential energy surface: advanced *ab initio* and density functional theory study, J. Mol. Struc. (THEOCHEM) 634 (2003) 127–135.

[19] X. B. Zhang, S. L. Zou, L. B. Harding, J. M. Bowman, A global *ab initio* potential energy surface for formaldehyde, J. Phys. Chem. A 108 (2004) 8980–8986.

[20] L. Koziol, Y. Wang, B. J. Braams, J. M. Bowman, A. I. Krylov, The theoretical prediction of infrared spectra of trans- and cis-hydroxycarbene calculated using full dimensional *ab initio* potential energy and dipole moment surfaces, J. Chem. Phys. 128 (2008) 204310.

[21] O. N. Ulenikov, E. S. Bekhtereva, C. Leroy, O. V. Gromova, A. L. Fomchenko, On the determination of the intramolecular potential energy surface of polyatomic molecules: hydrogen sulfide and formaldehyde as an illustration, J. Mol. Spectrosc. 255 (2009) 88–100.

[22] A. Yachmenev, S. N. Yurchenko, P. Jensen, W. Thiel, A new "spectroscopic" potential energy surface for formaldehyde in its ground electronic state, J. Chem. Phys. 134 (2011) 244307.

[23] P. R. Schreiner, H. P. Reisenauer, F. C. Pickard, A. C. Simmonett, W. D. Allen, E. Mátyus, A. G. Császár, Capture of hydroxymethylene and its fast disappearance through tunnelling, Nature 453 (2008) 906–909.

[24] P. Jankowski, A. McKellar, K. Szalewicz, Theory untangles the high-resolution infrared spectrum of the *ortho*-H_2CO van der Waals complex, Science 336 (2012) 1147–1150.

[25] D. Papp, T. Szidarovszky, A. G. Császár, A general variational approach for computing rovibrational resonances of polyatomic molecules. Application to the weakly bound H_2He^+ and H_2·CO systems, J. Chem. Phys. 147 (2017) 094106.

[26] H. Davy, Forms of miners' safety lamp, Philos. T. R. Soc. A 107 (1817) 77–86.

[27] P. Nau, J. Koppmann, A. Lackner, A. Brockhinke, Detection of formaldehyde in flames using UV and MIR absorption spectroscopy, Z. Phys. Chem. 229 (2015) 483–494.

[28] P. Fjodorow, O. Hellmig, V. M. Baev, H. B. Levinsky, A. V. Mokhov, Intracavity absorption spectroscopy of formaldehyde from 6230 to 6420 cm^{-1}, Appl. Phys. B 123 (2017) 147.

[29] Y. Ding, W. Y. Peng, C. L. Strand, R. K. Hanson, Quantitative measurements of broad-band mid-infrared absorption spectra of formaldehyde, acetaldehyde, and acetone at combustion-relevant temperatures near 5.7 μm, J. Quant. Spectrosc. Rad. Transf. 248 (2020) 106981.

[30] O. I. Korablev, M. Ackerman, V. A. Krasnopolsky, V. I. Moroz, C. Muller, A. V. Rodin, S. K. Aterya, Tentative identification of formaldehyde in the Martian atmosphere, Planet. Space Sci. 41 (1993) 441–451.

[31] D. Bockelee-Morvan, J. Crovisier, Formaldehyde in comets. II. Excitation of the rotational lines, Astron. Astrophys. 264 (1992) 282–291.

[32] S. N. Milam, A. J. Remijan, M. Womack, L. Abrell, L. M. Ziurys, S. Wyckoff, A. J. Apponi, D. N. Friedel, L. E. Snyder, J. M. Veal, P. Palmer, L. M. Woodney, M. F. A'Hearn, J. R. Forster, M. C. H. Wright, I. de Pater, S. Choi, M. Gesmundo, Formaldehyde in comets C/1995 O1 (Hale-Bopp), C/2002 T7 (LINEAR), and C/2001 Q4 (NEAT): investigating the cometary origin of H_2CO, Astrophys. J. 649 (2006) 1169.

[33] N. Dello Russo, R. J. Vervack, Jr., C. M. Lisse, H. A. Weaver, H. Kawakita, H. Kobayashi, A. L. Cochran, W. M. Harris, A. J. McKay, N. Biver, D. Bockelée-Morvan, J. Crovisier, The volatile composition and activity of comet 103P/Hartley 2 during the EPOXI closest approach, Astrophys. J. 734 (2011) L8.

[34] G. L. Villanueva, M. J. Mumma, M. A. Disanti, B. P. Bonev, E. L. Gibb, K. Magee-Sauer, G. A. Blake, C. Salyk, The molecular composition of Comet C/2007 W1 (Boattini): Evidence of a peculiar outgassing and a rich chemistry, Icarus 216 (2011) 227–240.

[35] B. A. Sargent, W. Forrest, D. M. Watson, P. d'Alessio, N. Calvet, E. Furlan, K. H. Kim, J. Green, K. Pontoppidan, I. Richter, C. Tayrien, Emission from water vapor and absorption from other gases at 5–7.5 μm in Spitzer-IRS spectra of protoplanetary disks, Astrophys. J. 792 (2014) 83.

[36] B. Zuckerman, D. Buhl, P. Palmer, L. E. Snyder, Observations of interstellar formaldehyde, Astrophys. J. 160 (1970) 485.

[37] J. G. Mangum, A. Wootten, R. L. Plambeck, The physical structure of Orion-KL on 2500-au scales using the K-doublet transitions of formaldehyde, Astrophys. J. 409 (1993) 282–298.

[38] J. R. Forster, W. M. Goss, T. L. Wilson, D. Downes, H. R. Dickel, A formaldehyde maser in NGC7538, Astron. Astrophys. 84 (1980) L1–L3.

[39] I. M. Hoffman, W. M. Goss, P. Palmer, The formaldehyde masers in Sgr B2: very long baseline array and very large array observations, Astrophys. J. 654 (2007) 971.

[40] J.-Z. Wang, Z.-Y. Zhang, Y. Gao, High resolution observations of the 6 cm H_2CO maser in NGC 6240, Res. Astron. Astrophys. 13 (2013) 270–276.

[41] S. Y. Parfenov, A. M. Sobolev, On the Class II methanol maser periodic variability due to the rotating spiral shocks in the gaps of discs around young binary stars, Mon. Not. R. Astron.

Soc. 444 (2014) 620–628.

[42] J. Terwisscha van Scheltinga, M. R. Hogerheijde, L. I. Cleeves, R. A. Loomis, C. Walsh, K. I. Oberg, E. A. Bergin, J. B. Bergner, G. A. Blake, J. K. Calahan, P. Cazzoletti, E. F. van Dishoeck, V. V. Guzman, J. Huang, M. Kama, C. Qi, R. Teague, D. J. Wilner, The TW Hya Rosetta Stone Project. II. Spatially Resolved Emission of Formaldehyde Hints at Low-temperature Gas-phase Formation, Astrophys. J. 906 (2021) 111. doi:{10.3847/1538-4357/abc9ba}.

[43] G. H. Dieke, G. B. Kistiakowsky, The structure of the ultraviolet absorption spectrum of formaldehyde. I, Phys. Rev. 45 (1934) 4–28.

[44] M.-C. Chuang, M. F. Foltz, C. B. Moore, T_1 barrier height, S_1–T_1 intersystem crossing rate, and S_0 radical dissociation threshold for H_2CO, D_2CO, and HDCO, J. Chem. Phys. 87 (1987) 3855.

[45] R. B. Lawrance, M. W. P. Strandberg, Centrifugal distortion in asymmetric top molecules. I. Ordinary formaldehyde, $H_2{}^{12}CO$, Phys. Rev. 83 (1951) 363–369.

[46] H. Takuma, T. Shimizu, K. Shimoda, Magnetic hyperfine spectrum of H_2CO by a maser, J. Phys. Soc. Jpn. 14 (1959) 1595–1599.

[47] T. Oka, Microwave spectrum of formaldehyde. II. Molecular structure in the ground state, J. Phys. Soc. Jpn. 15 (1960) 2274–2279.

[48] T. Oka, H. Hirakawa, K. Shimoda, Microwave spectrum of formaldehyde. I. K-type doubling spectra, J. Phys. Soc. Jpn. 15 (1960) 2265–2273.

[49] K. Shimoda, H. Takuma, T. Shimizu, Beam-type masers for radiofrequency spectroscopy, J. Phys. Soc. Jpn. 15 (1960) 2036–2041.

[50] L. Esterowitz, Rotational transitions and centrifugal distortion in uhf spectrum of formaldehyde, J. Chem. Phys. 39 (1963) 247.

[51] T. Shigenari, S. Kobayashi, H. Takuma, (6.3) rotational spectrum of H_2CO by a radiofrequency beam-type maser, J. Phys. Soc. Jpn. 18 (1963) 312–313.

[52] T. Oka, K. Takagi, Y. Morino, Microwave spectrum of formaldehyde in vibrationally excited states, J. Mol. Spectrosc. 14 (1964) 27–52.

[53] M. Takami, K-type doubling lines of H_2CO and HCOOH in the HF region, J. Phys. Soc. Jpn. 24 (1968) 372–376.

[54] T. Nakagawa, H. Kashiwagi, H. Kurihara, Y. Morino, Vibration-rotation spectra of formaldehyde, J. Mol. Spectrosc. 31 (1969) 436–450.

[55] A. F. Krupnov, L. I. Gershtein, V. G. Shustrov, V. V. Polyakov, Submillimeter microwave spectroscopy of formaldehyde, Opt. Spectrosc. 28 (1970) 257.

[56] K. D. Tucker, P. Thaddeus, G. R. Tomasevich, Precise laboratory measurement of 4830-MHz formaldehyde rotational transition, Astrophys. J. 161 (1970) L153–L154.

[57] T. Nakagawa, Y. Morino, Coriolis interactions in ν_4 and ν_6 bands of formaldehyde, J. Mol. Spectrosc. 38 (1971) 84–106.

[58] K. D. Tucker, G. R. Tomasevich, P. Thaddeus, Laboratory measurement of the 6 centimeter formaldehyde transitions, Astrophys. J. 169 (1971) 429–440.

[59] D. R. Johnson, F. J. Lovas, W. H. Kirchhoff, Microwave spectra of molecules of astrophysical interest: 1. Formaldehyde, formamide, and thioformaldehyde, J. Phys. Chem. Ref. Data 1 (1972) 1011–1046.

[60] R. B. Nerf, Laboratory measurement of millimeter-wavelength spectrum of formaldehyde,

Astrophys. J. 174 (1972) 467–468.

[61] K. D. Tucker, G. R. Tomasevich, P. Thaddeus, Laboratory measurement of the 2-centimeter, $2_{11} - 2_{12}$, transition of normal formaldehyde and its carbon-13 and oxygen-18 species, Astrophys. J. 174 (1972) 463–466.

[62] J. C. Chardon, D. Guichon, Structure hyperfine du spectre basse fréquence de H_2CO, J. Phys. (Paris) 34 (1973) 791–802.

[63] F. Y. Chu, S. M. Freund, J. W. C. Johns, T. Oka, $\Delta K = 2$ transitions in H_2CO and D_2CO, J. Mol. Spectrosc. 48 (1973) 328–335.

[64] J. W. C. Johns, A. R. W. McKellar, Stark spectroscopy with the CO laser: The ν_2 fundamentals of H_2CO and D_2CO, J. Mol. Spectrosc. 48 (1973) 354–371.

[65] R. A. Toth, High resolution measurements of the line positions and strengths of the $2\nu_2$ band of H_2CO, J. Mol. Spectrosc. 46 (1973) 470–489.

[66] R. B. Nerf, Pressure broadening and shift in the millimeter-wave spectrum of formaldehyde, J. Mol. Spectrosc. 58 (1975) 451–473.

[67] K. Tanaka, K. Yamada, T. Nakagawa, K. Kuchitsu, J. Overend, Infrared spectrum of formaldehyde: Coriolis interactions in the combination bands $\nu_2 + \nu_6$ and $\nu_2 + \nu_3$, J. Mol. Spectrosc. 54 (1975) 243–260.

[68] M. Allegrini, J. Johns, A. McKellar, A study of the Coriolis-coupled ν_4, ν_6, and ν_3 fundamental bands and the $\nu_5 \leftarrow \nu_6$ difference band of H_2CO; measurement of the dipole moment for $\nu_5 = 1$, J. Mol. Spectrosc. 67 (1977) 476–495.

[69] M. Allegrini, J. W. C. Johns, A. R. W. McKellar, Stark spectroscopy with the CO laser: the ν_3 fundamental band of H_2CO, J. Mol. Spectrosc. 66 (1977) 69–78.

[70] J. C. Chardon, D. Guichon, Spectre radiofréquence de H_2CO dans des états vibrationnels excités, J. Phys. (Paris) 38 (2) (1977) 113–120.

[71] B. Fabricant, D. Krieger, J. S. Muenter, Molecular beam electric resonance study of formaldehyde, thioformaldehyde, and ketene, J. Chem. Phys. 67 (1977) 1576–1586.

[72] D. Dangoisse, E. Willemot, J. Bellet, Microwave spectrum of formaldehyde and its isotopic species in D, ^{13}C, and ^{18}O: study of Coriolis resonance between ν_4 and ν_6 vibrational excited states, J. Mol. Spectrosc. 71 (1978) 414–429.

[73] A. S. Pine, Doppler-limited spectra of C–H stretching fundamentals of formaldehyde, J. Mol. Spectrosc. 70 (1978) 167–178.

[74] L. R. Brown, R. H. Hunt, A. S. Pine, Wavenumbers, line strengths, and assignments in the Doppler-limited spectrum of formaldehyde from 2700 cm^{-1} to 3000 cm^{-1}, J. Mol. Spectrosc. 75 (1979) 406–428.

[75] J. L. Hardvick, S. M. Till, Laser excited resonance fluorescence in formaldehyde, J. Chem. Phys. 70 (1979) 2340.

[76] R. Cornet, G. Winnewisser, A precise study of the rotational spectrum of formaldehyde $H_2{}^{12}C^{16}O$, $H_2{}^{13}C^{16}O$, $H_2{}^{12}C^{18}O$, $H_2{}^{13}C^{18}O$, J. Mol. Spectrosc. 80 (1980) 438–452.

[77] J.-C. Chardon, J.-J. Miller, Spectroscopie résonance électrique des jets moléculaires : formes des raies de résonance en présence d'effet Doppler, Can. J. Phys. 59 (1981) 378–386.

[78] D. M. Sweger, R. L. Sams, Diode laser spectra of the ν_2 band of $H_2{}^{12}CO$ and $H_2{}^{13}CO$, J. Mol. Spectrosc. 87 (1981) 18–28.

[79] C. Bréchignac, J. W. C. Johns, A. R. W. McKellar, M. Wong, The ν_2 fundamental band of H_2CO, J. Mol. Spectrosc. 96 (1982) 353–361.

[80] T. Tipton, J.-I. Choe, S. G. Kukolich, R. Hubbard, Fourier transform spectroscopy on the $3\nu_2$, $2\nu_2 + \nu_6$ and $\nu_3 + \nu_5$ bands of H_2CO, J. Mol. Spectrosc. 114 (1985) 239–256.

[81] S. Nadler, S. J. Daunt, D. C. Reuter, Tunable diode-laser measurements of formaldehyde foreign-gas broadening parameters and line strengths in the 9–11 μm region, Appl. Optics 26 (1987) 1641–1646.

[82] D. S. Cline, P. L. Varghese, High resolution spectral measurements in the ν_5 band of formaldehyde using a tunable IR diode laser, Appl. Optics 27 (1988) 3219–3224.

[83] D. C. Reuter, S. Nadler, S. J. Daunt, J. W. C. Johns, Frequency and intensity analysis of the ν_3 band, ν_4 band and ν_6 band of formaldehyde, J. Chem. Phys. 91 (1989) 646–654.

[84] F. Ito, T. Nakanaga, H. Takeo, FTIR spectra of the $2\nu_4$, $\nu_4+\nu_6$ and $2\nu_6$ bands of formaldehyde, Spectrochim. Acta A 50 (1994) 1397–1412.

[85] R. Bocquet, J. Demaison, L. Poteau, M. Liedtke, S. Belov, K. M. T. Yamada, G. Winnewisser, C. Gerke, J. Gripp, T. Köhler, The ground state rotational spectrum of formaldehyde, J. Mol. Spectrosc. 177 (1996) 154–159.

[86] P. Theulé, A. Callegari, T. R. Rizzo, J. S. Muenter, Fluorescence detected microwave Stark effect measurements in excited vibrational states of H_2CO, J. Chem. Phys. 119 (2003) 8910–8915.

[87] S. Nadler, D. C. Reuter, S. J. Daunt, J. W. C. Johns, The ν_3, ν_4 and ν_6 bands of formaldehyde: a spectral catalog from 900 to 1580 cm^{-1}, Nasa technical memorandum, NASA (1988).

[88] R. J. Bouwens, J. A. Hammerschmidt, M. M. Grzeskowiak, T. A. Stegink, P. M. Yorba, W. F. Polik, Pure vibrational spectroscopy of S_0 formaldehyde by dispersed fluorescence, J. Chem. Phys. 104 (1996) 460–479.

[89] D. Luckhaus, M. J. Coffey, M. D. Fritz, F. F. Crim, Experimental and theoretical vibrational overtone spectra of $v_{\mathrm{CH}} = 3, 4, 5$, and 6 in formaldehyde (H_2CO), J. Chem. Phys. 104 (1996) 3472–3478.

[90] H. Barry, L. Corner, G. Hancock, R. Peverall, G. A. D. Ritchie, Cross sections in the $2\nu_5$ band of formaldehyde studied by cavity enhanced absorption spectroscopy near 1.76 μm, Phys. Chem. Chem. Phys. 4 (2002) 445–450.

[91] S. Brünken, H. S. P. Müller, F. Lewen, G. Winnewisser, High accuracy measurements on the ground state rotational spectrum of formaldehyde (H_2CO) up to 2 THz, Phys. Chem. Chem. Phys. 5 (2003) 1515–1518.

[92] A. Perrin, F. Keller, J. M. Flaud, New analysis of the ν_2, ν_3, ν_4, and ν_6 bands of formaldehyde, $H_2{}^{12}C^{16}O$ line positions and intensities in the 5–10 μm spectral region, J. Mol. Spectrosc. 221 (2003) 192–198.

[93] M. Staak, E. W. Gash, D. S. Venables, A. A. Ruth, The rotationally-resolved absorption spectrum of formaldehyde from 6547 to 6804 cm^{-1}, J. Mol. Spectrosc. 229 (2005) 115–121.

[94] J. M. Flaud, W. J. Lafferty, R. L. Sams, S. W. Sharpe, High resolution spectroscopy of $H_2{}^{12}C^{16}O$ in the 1.9 to 2.56 μm spectral range, Mol. Phys. 104 (2006) 1891–1903.

[95] A. Perrin, A. Valentin, L. Daumont, New analysis of the $2\nu_4$, $\nu_4 + \nu_6$, $2\nu_6$, $\nu_3 + \nu_4$, $\nu_3 + \nu_6$, ν_1, ν_5, $\nu_2 + \nu_4$, $2\nu_3$, $\nu_2 + \nu_6$ and $\nu_2 + \nu_3$ bands of formaldehyde $H_2{}^{12}C^{16}O$: line positions and intensities in the 3.5μm spectral region, J. Mol. Struct. 780-781 (2006) 28–44.

[96] R. Perez, J. M. Brown, Y. Utkin, J. Han, R. F. Curl, Observation of hot bands in the infrared spectrum of H_2CO, J. Mol. Spectrosc. 236 (2006) 151–157.

[97] F. K. Tchana, A. Perrin, N. Lacome, New analysis of the ν_2 band of formaldehyde ($H_2{}^{12}C^{16}O$):

line positions for the ν_2, ν_3, ν_4 and ν_6 interacting bands, J. Mol. Spectrosc. 245 (2007) 141–144.

[98] W. Zhao, X. Gao, L. Deng, T. Huang, T. Wu, W. Zhang, Absorption spectroscopy of formaldehyde at 1.573 μm, J. Quant. Spectrosc. Rad. Transf. 107 (2007) 331–339.

[99] S. Saha, H. Barry, G. Hancock, G. A. D. Ritchie, C. M. Western, Rotational analysis of the $2\nu_5$ band of formaldehyde, Mol. Phys. 105 (2007) 797–805.

[100] L. Margulés, A. Perrin, R. Janeckova, S. Bailleux, C. P. Endres, T. F. Giesen, S. Schlemmer, Rotational transitions within the 2^1, 3^1, 4^1, and 6^1 states of formaldehyde $H_2{}^{12}C^{16}O$, Can. J. Phys. 87 (2009) 425–435.

[101] A. Perrin, D. Jacquemart, F. K. Tchana, N. Lacome, Absolute line intensities measurements and calculations for the 5.7 and 3.6 μm bands of formaldehyde, J. Quant. Spectrosc. Rad. Transf. 110 (2009) 700–716.

[102] J. Cihelka, I. Matulková, S. Civiš, Laser diode photoacoustic and FTIR laser spectroscopy of formaldehyde in the 2.3 μm and 3.5 μm spectral range, J. Mol. Spectrosc. 256 (2009) 68–74.

[103] D. Jacquemart, A. Laraia, F. K. Tchana, R. R. Gamache, A. Perrin, N. Lacome, Formaldehyde around 3.5 and 5.7 μm: measurement and calculation of broadening coefficients, J. Quant. Spectrosc. Rad. Transf. 111 (2010) 1209–1222.

[104] S. Eliet, A. Cuisset, M. Guinet, F. Hindle, G. Mouret, R. Bocquet, J. Demaison, Rotational spectrum of formaldehyde reinvestigated using a photomixing THz synthesizer, J. Mol. Spectrosc. 279 (2012) 12–15.

[105] A. A. Ruth, U. Heitmann, E. Heinecke, C. Fittschen, The rotationally-resolved absorption spectrum of formaldehyde from 6547 to 7051 cm^{-1}, Z. Phys. Chem. 229 (2015) 1609–1624.

[106] H. S. P. Müller, F. Lewen, Submillimeter spectroscopy of $H_2C^{17}O$ and a revisit of the rotational spectra of $H_2C^{18}O$ and $H_2C^{16}O$, J. Mol. Spectrosc. 331 (2017) 28–33.

[107] T. L. Tan, R. Ádawiah, L. L. Ng, The $2\nu_2$ bands of $H_2{}^{12}CO$ and $H_2{}^{13}CO$ by high-resolution FTIR spectroscopy, J. Mol. Spectrosc. 340 (2017) 16–20.

[108] T. Furtenbacher, A. G. Császár, J. Tennyson, MARVEL: measured active rotational-vibrational energy levels, J. Mol. Spectrosc. 245 (2007) 115–125.

[109] T. Furtenbacher, A. G. Császár, MARVEL: measured active rotational-vibrational energy levels. II. Algorithmic improvements, J. Quant. Spectrosc. Rad. Transf. 113 (2012) 929–935.

[110] R. Tóbiás, T. Furtenbacher, J. Tennyson, A. G. Császár, Accurate empirical rovibrational energies and transitions of $H_2{}^{16}O$, Phys. Chem. Chem. Phys. 21 (2019) 3473–3495.

[111] J. Tennyson, P. F. Bernath, L. R. Brown, A. Campargue, M. R. Carleer, A. G. Császár, R. R. Gamache, J. T. Hodges, A. Jenouvrier, O. V. Naumenko, O. L. Polyansky, L. S. Rothman, R. A. Toth, A. C. Vandaele, N. F. Zobov, L. Daumont, A. Z. Fazliev, T. Furtenbacher, I. E. Gordon, S. N. Mikhailenko, S. V. Shirin, IUPAC critical evaluation of the rotational-vibrational spectra of water vapor. Part I. Energy levels and transition wavenumbers for $H_2{}^{17}O$ and $H_2{}^{18}O$, J. Quant. Spectrosc. Rad. Transf. 110 (2009) 573–596.

[112] J. Tennyson, S. N. Yurchenko, ExoMol: molecular line lists for exoplanet and other atmospheres, Mon. Not. R. Astron. Soc. 425 (2012) 21–33.

[113] A. F. Al-Refaie, S. N. Yurchenko, A. Yachmenev, J. Tennyson, ExoMol line lists VIII: a variationally computed line list for hot formaldehyde, Mon. Not. R. Astron. Soc. 448 (2015) 1704–1714.

[114] J. L. Birkby, Spectroscopic direct detection of exoplanets, in: H. Deeg, J. Belmonte (Eds.), Handbook of exoplanets, Springer, New York, 2018, pp. 1485–1508.

[115] H. J. Hoeijmakers, R. J. de Kok, I. A. G. Snellen, M. Brogi, J. L. Birkby, H. Schwarz, A search for TiO in the optical high-resolution transmission spectrum of HD 209458b: hindrance due to inaccuracies in the line database, Astron. Astrophys. 575 (2015) A20.

[116] J. Tennyson, S. N. Yurchenko, A. F. Al-Refaie, V. H. J. Clark, K. L. Chubb, E. K. Conway, A. Dewan, M. N. Gorman, C. Hill, A. E. Lynas-Gray, T. Mellor, L. K. McKemmish, A. Owens, O. L. Polyansky, M. Semenov, W. Somogyi, G. Tinetti, A. Upadhyay, I. Waldmann, Y. Wang, S. Wright, O. P. Yurchenko, The 2020 release of the ExoMol database: molecular line lists for exoplanet and other hot atmospheres, J. Quant. Spectrosc. Rad. Transf. 255 (2020) 107228.

[117] A. G. Császár, T. Furtenbacher, Spectroscopic networks, J. Mol. Spectrosc. 266 (2011) 99–103.

[118] A. G. Császár, T. Furtenbacher, P. Árendás, Small molecules – big data, J. Phys. Chem. A 120 (2016) 8949–8969.

[119] P. Árendás, T. Furtenbacher, A. G. Császár, On spectra of spectra, J. Math. Chem. 54 (2016) 806–822.

[120] T. Furtenbacher, R. Tóbiás, J. Tennyson, O. L. Polyansky, A. G. Császár, W2020: A database of validated rovibrational experimental transitions and empirical energy levels of $H_2{}^{16}O$, J. Phys. Chem. Ref. Data 49 (2020) 033101.

[121] T. Furtenbacher, P. Árendás, G. Mellau, A. G. Császár, Simple molecules as complex systems, Sci. Rep. 4 (2014) 4654.

[122] R. Tóbiás, T. Furtenbacher, I. Simkó, A. G. Császár, M. L. Diouf, F. M. J. Cozijn, J. M. A. Staa, E. J. Salumbides, W. Ubachs, Spectroscopic-network-assisted precision spectroscopy and its application to water, Nat. Commun. 11 (2020) 1708.

[123] J. Tennyson, P. F. Bernath, L. R. Brown, A. Campargue, A. G. Császár, L. Daumont, R. R. Gamache, J. T. Hodges, O. V. Naumenko, O. L. Polyansky, L. S. Rothman, R. A. Toth, A. C. Vandaele, N. F. Zobov, S. Fally, A. Z. Fazliev, T. Furtenbacher, I. E. Gordon, S.-M. Hu, S. N. Mikhailenko, B. A. Voronin, IUPAC critical evaluation of the rotational-vibrational spectra of water vapor. Part II. Energy levels and transition wavenumbers for $HD^{16}O$, $HD^{17}O$, and $HD^{18}O$, J. Quant. Spectrosc. Rad. Transf. 110 (2010) 2160–2184.

[124] J. Tennyson, P. F. Bernath, L. R. Brown, A. Campargue, A. G. Császár, L. Daumont, R. R. Gamache, J. T. Hodges, O. V. Naumenko, O. L. Polyansky, L. S. Rothman, A. C. Vandaele, N. F. Zobov, A. R. A. Derzi, C. Fábri, A. Z. Fazliev, T. Furtenbacher, I. E. Gordon, L. Lodi, I. I. Mizus, IUPAC critical evaluation of the rotational-vibrational spectra of water vapor. Part III. Energy levels and transition wavenumbers for $H_2{}^{16}O$, J. Quant. Spectrosc. Rad. Transf. 117 (2013) 29–80.

[125] J. Tennyson, P. F. Bernath, L. R. Brown, A. Campargue, A. G. Császár, L. Daumont, R. R. Gamache, J. T. Hodges, O. V. Naumenko, O. L. Polyansky, L. S. Rothman, A.C.Vandaele, N. F. Zobov, N. Dénes, A. Z. Fazliev, T. Furtenbacher, I. E. Gordon, S.-M.Hu, T. Szidarovszky, I. A. Vasilenko, IUPAC critical evaluation of the rotational-vibrational spectra of water vapor. Part IV. Energy levels and transition wavenumbers for $D_2{}^{16}O$, $D_2{}^{17}O$, and $D_2{}^{18}O$, J. Quant. Spectrosc. Rad. Transf. 117 (2014) 93–108.

[126] J. Tennyson, P. F. Bernath, L. R. Brown, A. Campargue, A. G. Császár, L. Daumont, R. R. Gamache, J. T. Hodges, O. V. Naumenko, O. L. Polyansky, L. S. Rothman, A. C. Vandaele, N. F. Zobov, A database of water transitions from experiment and theory (IUPAC technical report), Pure Appl. Chem. 86 (2014) 71–83.

[127] T. Furtenbacher, I. Szabó, A. G. Császár, P. F. Bernath, S. N. Yurchenko, J. Tennyson, Experimental energy levels and partition function of the $^{12}C_2$ molecule, Astrophys. J. Suppl.

S. 224 (2016) 44.

[128] L. K. McKemmish, T. Masseron, S. Sheppard, E. Sandeman, Z. Schofield, T. Furtenbacher, A. G. Császár, J. Tennyson, C. Sousa-Silva, MARVEL analysis of the measured high-resolution rovibronic spectra of $^{48}Ti^{16}O$, Astrophys. J. Suppl. S. 228 (2017) 15.

[129] L. K. McKemmish, J. Borsovszky, K. L. Goodhew, S. Sheppard, A. F. V. Bennett, A. D. J. Martin, A. Singh, C. A. J. Sturgeon, T. Furtenbacher, A. G. Császár, J. Tennyson, MARVEL analysis of the measured high-resolution rovibronic spectra of $^{90}Zr^{16}O$, Astrophys. J. 867 (2018) 33.

[130] D. Darby-Lewis, H. Shah, D. Joshi, F. Khan, M. Kauwo, N. Sethi, P. F. Bernath, T. Furtenbacher, R. Tóbiás, A. G. Császár, J. Tennyson, MARVEL analysis of the measured high-resolution spectra of ^{14}NH, J. Mol. Spectrosc. 362 (2019) 69–76.

[131] L. K. McKemmish, A.-M. Syme, J. Borsovszky, S. N. Yurchenko, J. Tennyson, T. Furtenbacher, A. G. Császár, An update to the MARVEL data set and ExoMol line list for $^{12}C_2$, Mon. Not. R. Astron. Soc. 497 (2020) 1081–1097.

[132] T. Furtenbacher, T. Szidarovszky, C. Fábri, A. G. Császár, MARVEL analysis of the rotational-vibrational states of the molecular Ions H_2D^+ and D_2H^+, Phys. Chem. Chem. Phys. 15 (2013) 10181–10193.

[133] T. Furtenbacher, T. Szidarovszky, E. Mátyus, C. Fábri, A. G. Császár, Analysis of the rotational-vibrational states of the molecular ion H_3^+, J. Chem. Theor. Comput. 9 (2013) 5471–5478.

[134] K. L. Chubb, O. Naumenko, S. Keely, S. Bartolotto, S. MacDonald, M. Mukhtar, A. Grachov, J. White, E. Coleman, A. Liu, A. Z. Fazliev, E. R. Polovtseva, V.-M. Horneman, A. Campargue, T. Furtenbacher, A. G. Császár, S. N. Yurchenko, J. Tennyson, MARVEL analysis of the measured high-resolution rovibrational spectra of H_2S, J. Quant. Spectrosc. Rad. Transf. 218 (2018) 178–186.

[135] R. Tóbiás, T. Furtenbacher, A. G. Császár, O. V. Naumenko, J. Tennyson, J.-M. Flaud, P. Kumar, B. Poirier, Critical evaluation of measured rotational-vibrational transitions of four sulphur isotopologues of $S^{16}O_2$, J. Quant. Spectrosc. Rad. Transf. 208 (2018) 152–163.

[136] A. R. Al Derzi, T. Furtenbacher, S. N. Yurchenko, J. Tennyson, A. G. Császár, MARVEL analysis of the measured high-resolution spectra of $^{14}NH_3$, J. Quant. Spectrosc. Rad. Transf. 161 (2015) 117–130.

[137] K. L. Chubb, M. Joseph, J. Franklin, N. Choudhury, T. Furtenbacher, A. G. Császár, G. Gaspard, P. Oguoko, A. Kelly, S. N. Yurchenko, J. Tennyson, C. Sousa-Silva, MARVEL analysis of the measured high-resolution spectra of C_2H_2, J. Quant. Spectrosc. Rad. Transf. 204 (2018) 42–55.

[138] T. Furtenbacher, P. A. Coles, J. Tennyson, S. N. Yurchenko, S. Yu, B. Drouin, R. Tóbiás, A. G. Császár, Empirical rovibrational energy levels of ammonia up to 7500 cm^{-1}, J. Quant. Spectrosc. Rad. Transf. 251 (2020) 107027.

[139] C. Fábri, E. Mátyus, T. Furtenbacher, L. Nemes, B. Mihály, T. Zoltáni, A. G. Császár, Variational quantum mechanical and active database approaches to the rotational-vibrational spectroscopy of ketene, H_2CCO, J. Chem. Phys. 135 (2011) 094307.

[140] R. S. Mulliken, Report on notation for the spectra of polyatomic molecules, J. Chem. Phys. 23 (1955) 1997–2011.

[141] H. W. Kroto, Molecular rotation spectra, Dover, New York, 1992.

[142] M. Melosso, B. Conversazioni, C. Degli Esposti, L. Dore, E. Cané, F. Tamassia, L. Bizzocchi, The pure rotational spectrum of $^{15}ND_2$ observed by millimetre and submillimetre-wave spectroscopy, J. Quant. Spectrosc. Rad. Transf. 222 (2019) 186–189.

[143] C. Degli Esposti, M. Melosso, L. Bizzocchi, F. Tamassia, L. Dore, Determination of a semi-experimental equilibrium structure of 1-phosphapropyne from millimeter-wave spectroscopy of CH_3CP and CD_3CP, J. Mol. Struct. 1203 (2020) 127429.

[144] W. E. Lamb Jr., Theory of an optical maser, Phys. Rev. 134 (1964) A1429.

[145] M. Melosso, L. Dore, J. Gauss, C. Puzzarini, Deuterium hyperfine splittings in the rotational spectrum of NH_2D as revealed by Lamb-dip spectroscopy, J. Mol. Spectrosc. (2020) 111291.

[146] S. Carter, N. C. Handy, J. Demaison, The rotational levels of the ground vibrational state of formaldehyde, Mol. Phys. 90 (1997) 729–737.

[147] H. Takuma, K. M. Evenson, T. Shigenari, Zeeman effect and magnetic hyperfine structure in low frequency transitions of H_2CO, J. Phys. Soc. Jpn. 21 (1966) 1622–1623.

[148] G. Erlandsson, Millimeter wave spectrum of formaldehyde, J. Chem. Phys. 25 (1956) 579–580.

[149] T. Nakagawa, K. Yamada, K. Kuchitsu, Vibration-rotation spectrum of formaldehyde: C–H stretching fundamentals ν_1 and ν_5, J. Mol. Spectrosc. 63 (1976) 485–508.

[150] I. E. Gordon, M. R. Potterbusch, D. Bouquin, C. C. Erdmann, J. S. Wilzewski, L. S. Rothman, Are your spectroscopic data being used?, J. Mol. Spectrosc. 327 (2016) 232–238.

[151] I. E. Gordon, L. S. Rothman, C. Hill, R. V. Kochanov, Y. Tan, P. F. Bernath, M. Birk, V. Boudon, A. Campargue, K. V. Chance, B. J. Drouin, J.-M. Flaud, R. R. Gamache, J. T. Hodges, D. Jacquemart, V. I. Perevalov, A. Perrin, K. P. Shine, M.-A. H. Smith, J. Tennyson, G. C. Toon, H. Tran, V. G. Tyuterev, A. Barbe, A. G. Császár, V. M. Devi, T. Furtenbacher, J. J. Harrison, J.-M. Hartmann, A. Jolly, T. J. Johnson, T. Karman, I. Kleiner, A. A. Kyuberis, J. Loos, O. M. Lyulin, S. T. Massie, S. N. Mikhailenko, N. Moazzen-Ahmadi, H. S. P. Müller, O. V. Naumenko, A. V. Nikitin, O. L. Polyansky, M. Rey, M. Rotger, S. W. Sharpe, K. Sung, E. Starikova, S. A. Tashkun, J. V. Auwera, G. Wagner, J. Wilzewski, P. Wcisło, S. Yu, E. J. Zak, The HITRAN 2016 molecular spectroscopic database, J. Quant. Spectrosc. Rad. Transf. 203 (2017) 3–69.

[152] National Academies of Sciences, Engineering, and Medicine, Frequency allocations and spectrum protection for scientific uses, National Academies Press, Washington, 2015.

[153] M. J. Down, C. Hill, S. N. Yurchenko, J. Tennyson, L. R. Brown, I. Kleiner, Re-analysis of ammonia spectra: Updating the HITRAN $^{14}NH_3$ database, J. Quant. Spectrosc. Rad. Transf. 130 (2013) 260–272.

[154] V. Laporta, I. F. Schneider, J. Tennyson, Dissociative electron attachment cross sections for vibrationally excited NO molecule and N^- anion formation, Plasma Sources Sci. Technol. 20 (2020) 10LT01.

[155] J. Tennyson, C. Hill, S. N. Yurchenko, Data structures for ExoMol: Molecular line lists for exoplanet and other atmospheres, in: 6^{th} international conference on atomic and molecular data and their applications ICAMDATA-2012, Vol. 1545 of AIP Conference Proceedings, AIP, New York, 2013, pp. 186–195.

[156] O. L. Polyansky, A. A. Kyuberis, N. F. Zobov, J. Tennyson, S. N. Yurchenko, L. Lodi, ExoMol molecular line lists XXX: A complete high-accuracy line list for water, Mon. Not. R. Astron. Soc. 480 (2018) 2597–2608.

[157] S. N. Yurchenko, H. Williams, P. C. Leyland, L. Lodi, J. Tennyson, ExoMol line lists XXVIII:

the rovibronic spectrum of AlH, Mon. Not. R. Astron. Soc. 479 (2018) 1401–1411.

[158] L. K. McKemmish, T. Masseron, H. J. Hoeijmakers, V. Pérez-Mesa, S. L. Grimm, S. N. Yurchenko, J. Tennyson, ExoMol Molecular line lists – XXXIII. The spectrum of titanium oxide, Mon. Not. R. Astron. Soc. 488 (2019) 2836–2854.

[159] S. N. Yurchenko, T. M. Mellor, R. S. Freedman, J. Tennyson, ExoMol molecular line lists XXXIX: ro-vibrational molecular line list for CO_2, Mon. Not. R. Astron. Soc. 496 (2020) 5282–5291.

[160] S. N. Yurchenko, J. Tennyson, S. Miller, V. V. Melnikov, J. O'Donoghue, L. Moore, ExoMol molecular line lists XL: ro-vibrational molecular line list for the hydronium ion (H_3O^+), Mon. Not. R. Astron. Soc. 497 (2020) 2340–2351.

[161] P. A. Coles, S. N. Yurchenko, J. Tennyson, ExoMol molecular line lists XXXV: a rotation-vibration line list for hot ammonia, Mon. Not. R. Astron. Soc. 490 (2019) 4638–4647.